JGR Solid Earth

RESEARCH ARTICLE
10.1029/2023JB026740

The Impact of New Accelerometer Transplant Data (ACH) on GRACE Follow-On Along-Orbit Inter-Satellite Laser Ranging Observations and Monthly Time-Variable Gravity and Mascon Solutions

Khosro Ghobadi-Far[1], Susanna Werth[1], Manoochehr Shirzaei[1], Bryant D. Loomis[2], Thorben Döhne[3], Matthias O. Willen[3], and Martin Horwath[3]

[1]Department of Geosciences, Virginia Tech, Blacksburg, VA, USA, [2]Geodesy and Geophysics Laboratory, NASA Goddard Space Flight Center, Greenbelt, MD, USA, [3]Institut für Planetare Geodäsie, Technische Universität Dresden, Dresden, Germany

Abstract GRACE-D accelerometer data show significant bias jumps since one month after the launch of the GRACE Follow-On (GRACE-FO) satellites in May 2018, making them inapplicable for correcting GRACE-FO products for non-gravitational accelerations. The GRACE-FO Science Data System (SDS) compensated this issue by transplanting the GRACE-C accelerometer data toward that of GRACE-D. Recently, GRACE-FO SDS implemented an updated transplant method, used in the latest release of GRACE-FO data. Here, we examine the impact of updated accelerometer transplant data (ACH) on GRACE-FO measurements at all levels: (a) Level-1B inter-satellite laser ranging residuals measured along satellite orbit, (b) Level-2 time-variable gravity solutions from all SDS centers (JPL, CSR, and GFZ), and (c) Level-3 mascon solutions. We show that inter-satellite laser ranging residuals are modified at low frequencies below 1 mHz, affecting the along-orbit analysis of large-scale time-variable gravity signals. When mapped into monthly Level-2 spherical harmonic coefficients of geopotential, the low-frequency change in inter-satellite ranging residuals leads to substantial improvement of coefficients associated with resonant orders (i.e., 15, 30, 45, etc.) and C_{30}. We also present an improved SLR-derived C_{30} which significantly improves the agreement with updated GRACE-FO C_{30} at seasonal and interannual timescales. Moreover, we demonstrate the noise reduction in mass change estimates from new GRACE-FO Level-2 data over oceans, Greenland, and Antarctica for all SDS solutions. GRACE-FO mascon solutions show a moderate change in the updated release. Our comprehensive analyses demonstrate high-quality estimates of non-gravitational accelerations by the updated transplant method, resulting in more accurate GRACE-FO time-variable gravity and mass change observations.

Plain Language Summary GRACE Follow-On (GRACE-FO) consists of two satellites that orbit around the Earth at ~500 km altitude, following each other at a distance of ~200 km. The inter-satellite distance between the two satellites changes because of the gravitational as well as non-gravitational forces (e.g., air drag), and it is measured by high-precision sensors. To estimate time-variable gravity caused by mass change in the Earth system from inter-satellite ranging data, the effect of non-gravitational forces is reduced using on-board accelerometer measurements. The accelerometer on-board the GRACE-D satellite started to return erroneous measurements about 1 month after the launch. The GRACE-FO Science Data System (SDS) compensated this issue by transplanting the GRACE-C accelerometer data toward that of GRACE-D. An updated transplant accelerometer data set for GRACE-D was recently released by the GRACE-FO SDS and, consequently, new time-variable gravity and mass change solutions were released. In this paper, we demonstrate the improved accuracy of the new GRACE-FO time-variable gravity and mass change solutions caused by high-quality estimates of non-gravitational accelerations by the updated transplant method.

Key Points:

- GRACE Follow-On (GRACE-FO) laser ranging residuals are modified at low frequencies by ACH, affecting the along-orbit analysis of large-scale mass changes
- Geopotential spherical harmonic coefficients associated with resonant orders (i.e., ~15, 30, 45, etc.) show the largest improvement by ACH
- Monthly gravity fields show significantly lower noise for months when the angle between GRACE-FO orbital plane and Sun-Earth direction is ~0

Supporting Information:

Supporting Information may be found in the online version of this article.

Correspondence to:

K. Ghobadi-Far,
khosro@vt.edu

Citation:

Ghobadi-Far, K., Werth, S., Shirzaei, M., Loomis, B. D., Döhne, T., Willen, M. O., & Horwath, M. (2023). The impact of new accelerometer transplant data (ACH) on GRACE Follow-On along-orbit inter-satellite laser ranging observations and monthly time-variable gravity and mascon solutions. *Journal of Geophysical Research: Solid Earth*, *128*, e2023JB026740. https://doi.org/10.1029/2023JB026740

Received 14 MAR 2023
Accepted 6 JUN 2023

Author Contributions:

Conceptualization: Khosro Ghobadi-Far
Formal analysis: Khosro Ghobadi-Far, Susanna Werth, Manoochehr Shirzaei, Bryant D. Loomis, Thorben Döhne, Matthias O. Willen, Martin Horwath
Investigation: Khosro Ghobadi-Far, Susanna Werth, Manoochehr Shirzaei, Bryant D. Loomis, Thorben Döhne, Matthias O. Willen, Martin Horwath

1. Introduction

The Gravity Recovery and Climate Experiment (GRACE; Tapley et al., 2004) and its successor, the GRACE Follow-On (GRACE-FO; Landerer et al., 2020) satellite missions have been providing invaluable data since 2002 for monitoring the mass change at regional to global scales in various components of the Earth system such as oceans (Chen et al., 2019), cryosphere (e.g., Shepherd et al., 2018, 2020), hydrosphere (e.g., Rodell et al., 2018) and solid Earth (e.g., Han et al., 2006). GRACE and GRACE-FO have also played a vital role in understanding

Methodology: Khosro Ghobadi-Far, Susanna Werth, Manoochehr Shirzaei, Bryant D. Loomis, Thorben Döhne, Matthias O. Willen, Martin Horwath
Project Administration: Susanna Werth, Manoochehr Shirzaei
Supervision: Khosro Ghobadi-Far, Susanna Werth, Manoochehr Shirzaei, Martin Horwath
Validation: Bryant D. Loomis
Visualization: Khosro Ghobadi-Far, Susanna Werth, Manoochehr Shirzaei, Bryant D. Loomis, Thorben Döhne, Matthias O. Willen, Martin Horwath
Writing – original draft: Khosro Ghobadi-Far, Thorben Döhne, Matthias O. Willen
Writing – review & editing: Khosro Ghobadi-Far, Susanna Werth, Manoochehr Shirzaei, Bryant D. Loomis, Thorben Döhne, Matthias O. Willen, Martin Horwath

the impact of climate change (Tapley et al., 2019). The conventional mass change data products from GRACE and GRACE-FO used for Earth system monitoring are given as global snapshots (or maps) of gridded mass variations with monthly sampling, that is, Level-3 (L3) data products. They are computed either from monthly time-variable gravity solutions, given in terms of spherical harmonic (SH) coefficients of geopotential to a maximum degree and order like 60 (i.e., Level-2 [L2] data products) following Wahr et al. (1998) or directly from Level-1B (L1B) observations of inter-satellite tracking, orbit, orientation, and non-gravitational accelerations measured by on-board accelerometers (Loomis, Luthcke, & Sabaka, 2019; Save et al., 2016; Watkins et al., 2015). The L3 mass change data products derived directly from L1B measurements are usually referred to as the mass concentration (mascon) solutions. Official L2 data products are released by the GRACE-FO Science Data System (SDS) teams, which include the NASA Jet Propulsion Laboratory (JPL; Yuan, 2019; see https://dx.doi.org/10.5067/GFL20-MJ061), the Center for Space Research at the University of Texas at Austin (CSR; Yuan, 2019; see https://dx.doi.org/10.5067/GFL20-MC061), and the German Research Center for Geosciences (GFZ; Dahle et al., 2019; see https://doi.org/10.5880/GFZ.GRACEFO_06_GSM). The accuracy of L2 time-variable gravity and L3 mass change solutions depends on the data quality from the accelerometers on-board both satellites that are used for reducing the effect of non-gravitational accelerations acting on the satellites caused by, for example, air drag and solar-radiation pressure. The higher the accuracy of non-gravitational accelerations, the better the quality of resultant time-variable gravity and mass change data.

Since the launch of GRACE-FO, accelerometers on-board both of the satellites, namely, GRACE-C and GRACE-D, return spurious measurements associated with two types of high-frequency signals: (a) improper response at thruster firings and (b) the so-called Phantom Accelerations (McCullough et al., 2019). The Phantom Accelerations indicate large, spurious measurements in the accelerometer data, which show geographical correlations as well as correlation with the β' angle, and are not concurrent with the thruster firings (McCullough et al., 2019). β' is defined as the angle between the satellite's orbital plane and Sun-Earth direction, and in the case of GRACE-FO, it has a cycle of 161 days. To correct the spurious, high-frequency accelerometer measurements, the GRACE-FO SDS teams (a) remove the Phantom Accelerations by applying a threshold and then using linear interpolation to replace them and (b) makes use of a thrust model to replace the accelerometer data near the long thruster firings, which are planned thruster calibration maneuvers (McCullough et al., 2019). The thrust model is computed from the regression of accelerometer data over long thruster firings.

In addition to the spurious, high-frequency measurements, the GRACE-D accelerometer shows significant bias jumps since after about 1 month in orbit, starting from 21 June 2018. The GRACE-FO SDS centers used the GRACE-C accelerometer data to replace that of GRACE-D using the so-called transplant approach. This situation has occurred previously, during two periods of the GRACE mission's lifetime: (a) several weeks in 2002 and 2003 when only single accelerometer data from GRACE-A was available (Save et al., 2006) and (b) last several months at the end of the GRACE mission in 2017 when the GRACE-B accelerometer was turned off due to reduced battery load (Bandikova et al., 2019). Due to the along-track geometry and relatively small inter-satellite baseline of ∼200 km, both satellites of the twin-satellite missions GRACE and GRACE-FO pass over approximately the same location after a time interval of 20–30 s. As such, a transplant technique based on simple attitude and time corrections provides good results, as Save et al. (2006) demonstrated. However, in addition to the non-gravitational accelerations acting on the satellite, the on-board accelerometers also measure the effects of spacecraft operations, such as the residual linear accelerations due to thruster firing (Bandikova et al., 2019; Flury et al., 2008). These residual linear accelerations need to be accounted for in the transplant technique. Bandikova et al. (2019) introduced an improved accelerometer transplant approach by modeling the residual linear accelerations due to thruster firings, which resulted in enhanced GRACE L2 solutions with lower noise.

The official accelerometer data used for GRACE-FO gravity field processing are called ACT, and they are computed using the transplant technique by Bandikova et al. (2019) for all days starting from 21 June 2018, in addition to correcting for the Phantom Accelerations and accelerations at thrust firings (Harvey et al., 2022). The ACT data were applied for the SDS GRACE-FO L2 solutions published as data release 6 (RL06). The inefficacies in ACT data, in particular, adversely affect the low-degree geopotential SH coefficient $\overline{C}_{30}$ in the GRACE-FO RL06 solutions. Hence, the recommendation from SDS teams is to replace the GRCAE-FO $\overline{C}_{30}$ coefficient with values estimated from Satellite Laser Ranging (SLR) satellites (Loomis et al., 2020), as provided in Technical Note 14 (TN-14). Behzadpour et al. (2021) presented an alternative accelerometer transplant technique incorporating models for non-gravitational forces such as air drag and solar radiation pressure. The ITSG-Grace2018 solutions from Graz University of Technology (Kvas et al., 2019) based on this alternative transplant technique

show a better agreement with SLR-derived $\overline{C}_{20}$ and $\overline{C}_{30}$ compared to the values from SDS solutions (Behzadpour et al., 2021).

Recently, GRACE-FO SDS teams released a new accelerometer transplant data called ACH, which also incorporates the GRACE-D accelerometer data to further improve the corrections for solar radiation and Earth radiation pressure forces (McCullough, Harvey, et al., 2022). Thus, it is referred to as a hybrid-transplant accelerometer approach. Accordingly, the SDS teams published updated GRACE-FO solutions based on the ACH data as data release 6.1 (RL06.1). The GRACE-FO SDS teams encouraged the community to assess the impact of the ACH data on GRACE-FO time-variable gravity and mass change solutions and provide feedback (Landerer et al., 2022; McCullough, Fahnestock, et al., 2022). This is particularly important as the drag environment of the GRACE-FO satellites evolves with changes in the solar cycle and altitude decay (Landerer et al., 2022).

This paper responds to this call by presenting a comprehensive assessment of the impact of new accelerometer transplant data ACH on GRACE-FO measurements at all levels: (a) L1B inter-satellite ranging residuals from the Laser Ranging Interferometer (LRI, Abich et al., 2019), (b) L2 time-variable gravity solutions from all three SDS teams (JPL, CSR, and GFZ), and (c) L3 mass change solutions. In the case of L2 data, we present a comprehensive comparison of RL06 and RL06.1 solutions based on various analyses in the frequency, time and space domains and through comparison with independent data sets. In the case of L3 data, we examine the mascon solutions from JPL (Watkins et al., 2015) and NASA Goddard Space Flight Center (GSFC; Loomis, Luthcke, & Sabaka, 2019), which are directly computed from L1B data, as well as the L3 gridded mass change data from GFZ (Boergens et al., 2022; Sasgen et al., 2019; see http://gravis.gfz-potsdam.de/home), which are computed from L2 data. While monthly L2 and L3 data observe slowly varying mass changes in the Earth system, the along-orbit analysis of inter-satellite tracking data has helped to broaden the applications of GRACE/GRACE-FO to rapid mass and gravity changes associated with various processes like Earth's free oscillations (Ghobadi-Far, Han, et al., 2019), tsunamis (Ghobadi-Far, Han, Allgeyer, et al., 2020), floods (Han, Ghobadi-Far, et al., 2021, Han, Yeo, et al., 2021), and oceanic gyres (Ghobadi-Far et al., 2022). Thus, we decided to include the inter-satellite laser ranging residuals in addition to the more frequently used L2 and L3 data to thoroughly assess the ACH impact on the GRACE-FO observations at all levels.

This paper is organized as follows. Section 2 examines the change in GRACE-FO inter-satellite laser ranging residuals caused by ACH. Quantification of the ACH impact on GRACE-FO L2 data from JPL, CSR and GFZ through comparison of RL06 and RL06.1 solutions is presented in Section 3. Section 4 analyses the ACH impact on the mascon solutions from NASA JPL (Watkins et al., 2015) and GSFC (Loomis, Luthcke, & Sabaka, 2019) and L3 gridded mass change data from GFZ. Conclusions are presented in the last section.

2. Impact of ACH on GRACE-FO Inter-Satellite Laser Ranging Residuals

GRACE-FO is equipped with two inter-satellite tracking sensors: (a) a microwave-based K-band ranging (KBR) and (b) a LRI. The latter serves as a technology demonstration element of the mission to be used for future GRACE-like gravimetry missions (Landerer et al., 2020). Compared to KBR, the GRACE-FO LRI improves the gravitational perturbation measurements by ~1 order of magnitude at high frequencies above 10 mHz, which makes it more suitable for along-orbit analysis of time-variable gravity signals (Ghobadi-Far, Han, McCullough, et al., 2020).

We computed two sets of dynamic orbits of the GRACE-FO satellites by numerical integration using the background force models of the Earth's static gravity field model GGM05C (Ries et al., 2016), solid Earth and ocean tides, solid Earth and ocean pole tides, atmosphere and ocean de-aliasing L1B (AOD1B; Dobslaw et al., 2017), a time-variable gravity model representing trend and annual variability (obtained from GRACE and GRACE-FO), and non-gravitational accelerations based on the original (ACT1B) and updated (ACH1B) L1B accelerometer transplant data (see Loomis, Luthcke, and Sabaka (2019) for more details). Moreover, the following empirical parameters were incorporated in this processing step: state vectors of the two satellites, accelerometers biases and scales in all three directions every 90 min, empirical accelerations at 1 cycle-per-revolution in all three directions every 90 min, and a bias, trend and 1 cycle-per-revolution periodic signal applied to inter-satellite range-rate data every 180 min. We then calculated two sets of reference range-rate data sets from the dynamic orbits associated with ACT and ACH. The LRI range-rate residuals were then obtained by subtracting the reference range-rate from the measured values. Such range-rate residuals are the basis of GRACE and GRACE-FO data processing

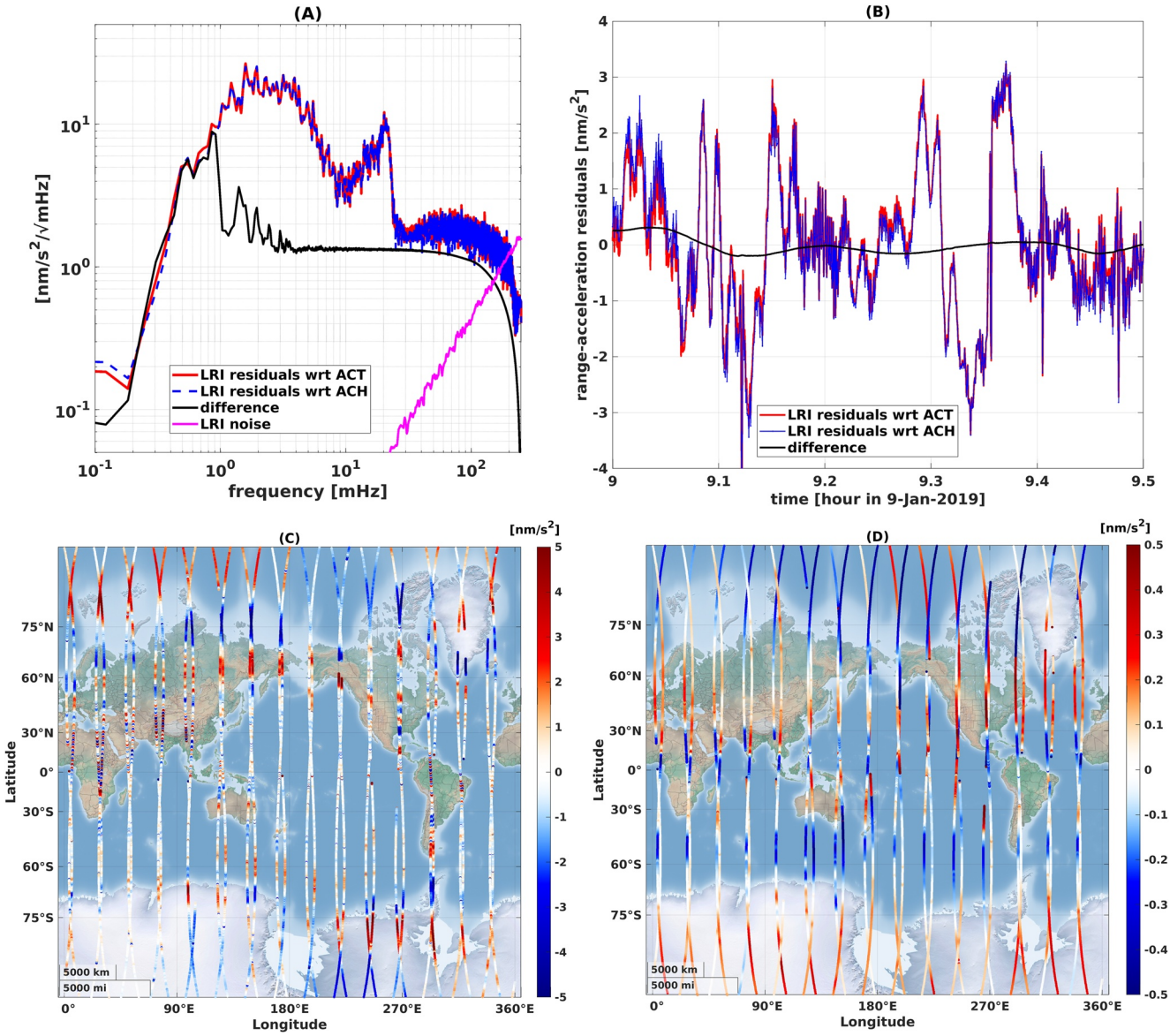

Figure 1. Impact of the new accelerometer transplant data ACH on GRACE-FO laser ranging interferometer (LRI) ranging residuals. (a) Amplitude spectral density of GRACE-FO LRI range-acceleration residuals with respect to ACT (red), ACH (blue) as well as their difference (black). The LRI noise from Abich et at. (2019) is also shown. (b) Timeseries of LRI range-acceleration residuals with respect to ACT (red), ACH (blue) as well as their difference (black) for a 30 min arc along the GRACE-FO orbit on 9 January 2019. (c) Spatial map of GRACE-FO LRI range-acceleration residuals with respect to ACT. (d) Spatial map of difference of GRACE-FO LRI range-acceleration residuals referenced to ACH and ACT. Results are based on LRI data on 9 January 2019. ACH modifies the GRACE-FO along-orbit gravity observations from inter-satellite LRI tracking at low frequencies below 1 mHz.

for estimating the monthly gravity field and mascon solutions. Since range-accelerations are more localized in space and, thus, better co-locate with the causative mass change (Ghobadi-Far et al., 2018; Ray et al., 2009), we performed our analyses based on the range-acceleration residuals obtained by numerical differentiation of range-rate residuals. We compared the range-acceleration residuals referenced to ACT and ACH in the frequency, time and space domains to evaluate the impact of the new accelerometer transplant data on instantaneous along-orbit gravitational observations from the GRACE-FO LRI.

Figure 1a shows the amplitude spectral density of LRI range-acceleration residuals with respect to ACT and ACH, as well as their difference (ACH-ACT) for data on 9 January 2019. The LRI sensor noise (Abich et al., 2019) is also shown. The spectrum of LRI residuals is dominated by time-variable gravity signals at frequencies below 10 mHz and by residual static gravity signals, due to errors in the background model GGM05C, over the frequency band

~10–25 mHz (Ghobadi-Far, Han, McCullough, et al., 2020). The update by the new accelerometer transplant data ACH is manifested in the LRI residuals at low frequencies below 1 mHz or 5 cycle-per-revolution (CPR), equivalent to spatial scales larger than 8,000 km. The timeseries of LRI range-acceleration residuals shown in Figure 1b consistently indicates the long-wavelength nature of the update by ACH.

The spatial map of the LRI range-acceleration residuals referenced to ACT shown in Figure 1c illustrates low-frequency time-variable gravity signals above regions with expected mass change like Greenland and Antarctica, as well as high-frequency static gravity signals over regions like the Himalayas and Africa, where the GGM05C model is erroneous (Ghobadi-Far, Han, McCullough, et al., 2020). The difference in LRI residuals between ACT and ACH indicates the modification of large-scale spatial variability of along-orbit time-variable gravity signals due to the update by ACH (see Figure 1d), consistent with the frequency and time domain analyses. The change in low-frequency or large-scale spatial components of LRI residuals mainly affects the analysis of phenomena with long-wavelength features like gravity changes caused by Earth's free oscillations (Ghobadi-Far, Han, et al., 2019) and the impact of seawater variable density on computing geopotential from ocean tides (Han et al., 2020).

The temporal and spatial inspection of the LRI range-acceleration residuals indicates that the magnitude of the update by ACH is ~0.5 nm/s^2. We note that the magnitude of the update increases in times with near-zero β' angle. For example, in April 2019, with $\beta' \cong 0$, the magnitude of the update increases to ~1 nm/s^2 (not shown). Moreover, the amplitude of the update could vary depending on the details of the dynamic orbit computation, particularly the incorporated empirical parameters, which mainly affect the low-frequency part of the spectrum. However, we emphasize that low-frequency dominance of the ACH update does not depend on the processing details. For example, the change in low-frequency part of the inter-satellite ranging residuals caused by updating the accelerometer data can be seen in Figure 14 of Behzadpour et al. (2021) as well. The impact of ACH on the KBR inter-satellite ranging residuals is similar to that of LRI, as the main difference between measurements from these two sensors occurs at high frequencies (Ghobadi-Far, Han, McCullough, et al., 2020).

3. Comparison of GRACE-FO Level-2 Time-Variable Gravity Solutions: RL06 Versus RL06.1

GRACE-FO L2 data from SDS teams represent monthly mean time-variable gravity fields, expressed as geopotential SH coefficients to the maximum degree 60 and 96 (Yuan, 2019). By comparing RL06 (computed from ACT) and RL06.1 (computed from ACH) L2 solutions from June 2018 to July 2022, we examined the impact of ACH on (a) low-degree SH coefficients $\overline{C}_{20}$ and $\overline{C}_{30}$ (Section 3.1), (b) the complete set of SH coefficients from degree 2 to 96 (Section 3.2), (c) noise reduction of mass change data in space and time domains (Section 3.3), and (d) ice-sheet mass change in Greenland and Antarctica (Section 3.4).

3.1. Geopotential Coefficients $\overline{C}_{20}$ and $\overline{C}_{30}$

The accelerometer error is dominant at the low-frequency band of the spectrum of inter-satellite ranging residuals, which leads to large errors in GRACE/GRACE-FO estimates of low-degree zonal SH coefficients $\overline{C}_{20}$ and $\overline{C}_{30}$ (e.g., Kim, 2000). Consequently, the update in low-frequency content of inter-satellite ranging residuals from the new accelerometer transplant data ACH should result in improved estimates of these geopotential coefficients. We compared the GRACE-FO $\overline{C}_{20}$ and $\overline{C}_{30}$ with SLR-derived values provided in the current version 2 of the TN-14 (Loomis et al., 2020; available at ftp://isdcftp.gfz-potsdam.de/grace-fo/DOCUMENTS/TECHNICAL_NOTES) to examine their improvement by ACH. As stated earlier, the GRACE-FO SDS recommends replacing these two coefficients in the GRACE-FO L2 data with those provided in TN-14.

We compared $\Delta\overline{C}_{20}$ ($=\overline{C}_{20}^{\mathrm{GRACE-FO}} - \overline{C}_{20}^{\mathrm{GGM05C}}$) timeseries from GRACE-FO RL06 and RL06.1 solutions with SLR values from the TN-14 for the solutions of JPL (Figure 2a), CSR (Figure 2b) and GFZ (Figure 2c). Figure 2 also shows the GRACE-FO β' angle. The largest deviation of GRACE-FO $\overline{C}_{20}$ from the SLR reference values happens at times with near-zero β' angle. That is because, during these times, GRACE-FO satellites are exposed to direct sunlight for half of the orbital revolution, while for the other half, they pass over the Earth's shadow, causing large temperature changes which consequently results in large variation in non-gravitational accelerations over each revolution (~90 min). In general, we see that GRACE-FO $\overline{C}_{20}$ estimates from RL06.1 are still

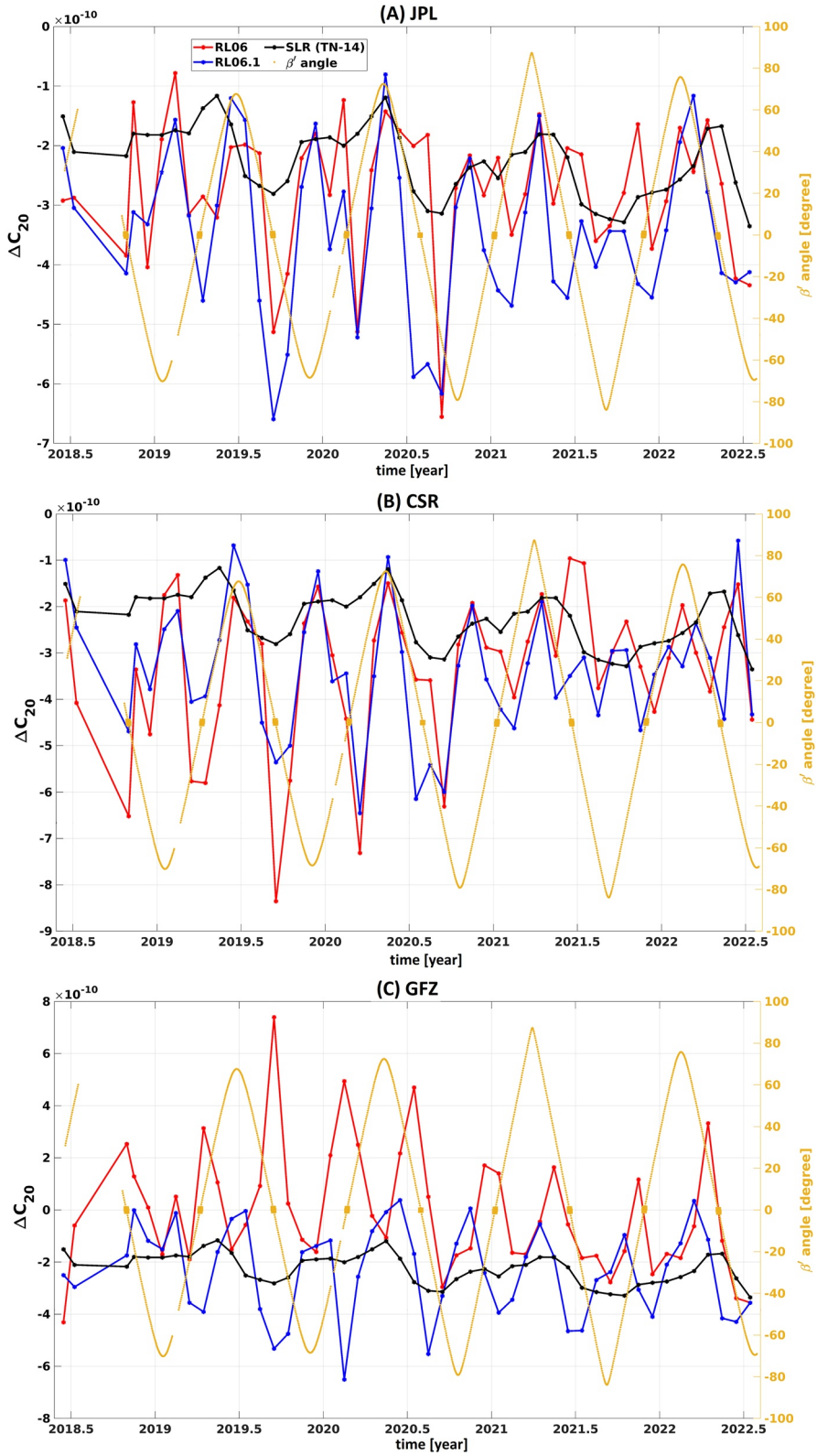

Figure 2. Impact of ACH on $\overline{C}_{20}$. Comparison of the $\Delta\overline{C}_{20}$ geopotential spherical harmonic coefficient from GRACE-FO (a) JPL, (b) CSR and (c) GFZ RL06 (red) and RL06.1 (blue) and Satellite Laser Ranging (SLR) (black) as provided in the current version 2 of TN-14. GRACE-FO β' angle (yellow) is also shown. RL06 and RL06.1 solutions are based on accelerometer transplant data ACT and ACH, respectively. The largest deviation from SLR reference values happens at times with near-zero β' angle.

significantly different from the SLR reference values. Among the three SDS solutions, GFZ RL06.1 shows the largest improvement with respect to RL06.

GRACE-FO and SLR estimates of $\Delta\overline{C}_{30}$ (illustrated by solid lines) are shown in Figures 3a–3c for JPL, CSR and GFZ solutions, respectively. The improvement by ACH reflected in RL06.1 estimates is visible for all three SDS solutions and they are the largest for periods with near-zero β' angle, when RL06 $\overline{C}_{30}$ estimates show the largest deviation from SLR values. We also examined the annual cycle of the timeseries of GRACE-FO and SLR $\Delta\overline{C}_{30}$ to quantify the improvement at the seasonal timescale (dashed lines in Figure 3). Table 1 reports the values of annual amplitude and phase for various $\Delta\overline{C}_{30}$ estimates, indicating that the phase of the annual cycle of GRACE-FO RL06.1 $\overline{C}_{30}$ estimates is significantly improved when compared with SLR. Annual phase computed from JPL, CSR and GFZ $\overline{C}_{30}$ timeseries changes from values of 259.21°, 250.74°, and 265.21° in the case of RL06 to 288.40°, 284.45° and 288.48° in the case of RL06.1, respectively, with the latter being closer to the SLR value of 292.53°. JPL and GFZ solutions show the best agreement with SLR in terms of the phase of annual cycle. The annual amplitude of the $\overline{C}_{30}$ timeseries is also slightly improved by the RL06.1 of all three solutions (see Table 1).

To accentuate the agreement between GRACE-FO RL06.1 and SLR $\overline{C}_{30}$ estimates at interannual timescales, we removed the mean annual cycle shown in dashed lines in Figure 3 from the original timeseries. Solid blue and black lines in Figure 4 show the deseasonalized timeseries of $\Delta\overline{C}_{30}$ from GRACE-FO RL06.1 and SLR, respectively, and the dashed blue and black lines show the linear trend of $\Delta\overline{C}_{30}$ timeseries. This analysis reveals a notable discrepancy in terms of interannual variability between GRACE-FO RL06.1 and SLR $\overline{C}_{30}$ timeseries. The linear trend of $\Delta\overline{C}_{30}$ timeseries from RL06.1 provided by JPL, CSR, and GFZ solutions is −1.41E−11, −1.50E−11, −1.60E−11, respectively, which is one order of magnitude larger than the SLR trend of −3.79E−12 (see Table 1). Any notable change in $\overline{C}_{30}$ would, among others, significantly affect mass balance estimates of Antarctica Ice-Sheets. This can be seen from the isolated mass effect of $\Delta\overline{C}_{30}$ displayed in Figure S1 of Supporting Information S1 and it was discussed by Loomis et al. (2020). Thus, it is worth further investigation, which is presented in Section 3.4.

Loomis et al. (2020) demonstrated the validity of SLR $\overline{C}_{30}$ estimates for the period after the launch of LARES in 2012. They showed that including a high-quality background time-variable gravity model in the SLR data processing plays a vital role in the accurate estimation of $\overline{C}_{20}$ and $\overline{C}_{30}$ (see also Loomis, Rachlin, & Luthcke, 2019). The currently used version 2 of TN-14 makes use of a regression model containing trend and annual terms up to degree/order 10 (only retaining terms with statistical significance) from GRACE and GRACE-FO RL06 data through October 2019. We computed a new test release for version 3 of TN-14 by updating the background time-variable gravity used in the SLR data processing based on the GRACE and GRACE-FO RL06 solutions to degree/order 60 until July 2022. The updated SLR processing changes the linear trend of $\overline{C}_{30}$ timeseries from −3.79E−12 to −1.19E−11, which is closer to the GRACE-FO RL06.1 estimates (see Table 1). The deseasonalized timeseries and linear trend computed from updated SLR $\overline{C}_{30}$ estimates are shown in Figure 4 in solid and dashed magenta lines, respectively. The agreement between GRACE-FO and the updated SLR $\overline{C}_{30}$ estimates in Figure 4 demonstrates the accurate representation of interannual variability of this geopotential coefficient in RL06.1 solutions. We note that using the GRACE and GRACE-FO RL06.1 solutions (instead of RL06) to degree/orer 60 as the background time-variable gravity model in the SLR data processing leads to similar $\overline{C}_{30}$ estimates (not shown).

We further validated the interannual variability of updated SLR $\overline{C}_{30}$ timeseries through comparison with GRACE-FO $\overline{C}_{30}$ estimates from ITSG-Grace2018 solutions, which are based on their own in-house accelerometer transplant data (Behzadpour et al., 2021; see Figure S2 in Supporting Information S1). Moreover, the statistical significance of the difference between the linear trend of $\overline{C}_{30}$ from GRACE-FO RL06.1 and SLR estimates is presented in Text S1 of Supporting Information S1.

We note that similar to the SLR $\overline{C}_{30}$ estimates provided by the current version 2 of TN-14, the annual cycle of the updated SLR $\overline{C}_{30}$ timeseries also agrees well with GRACE-FO RL06.1 (see Figure S3 in Supporting Information S1). Updating the background time-variable gravity in the SLR data processing further reduces the difference between the annual phase of GRACE-FO RL06.1 and SLR $\overline{C}_{30}$ timeseries from ∼4 to ∼1° (see Table 1). This indicates a significant improvement in the GRACE-FO RL06.1 $\overline{C}_{30}$ estimates thanks to the new accelerometer transplant data ACH.

3.2. Spectral Analysis of Level-2 Spherical Harmonic Solutions

We extended our analysis of L2 solutions from low-degree harmonics to the whole set of SH coefficients to examine the improvement by ACH on the full spectrum of time-variable gravity measured by the GRACE-FO

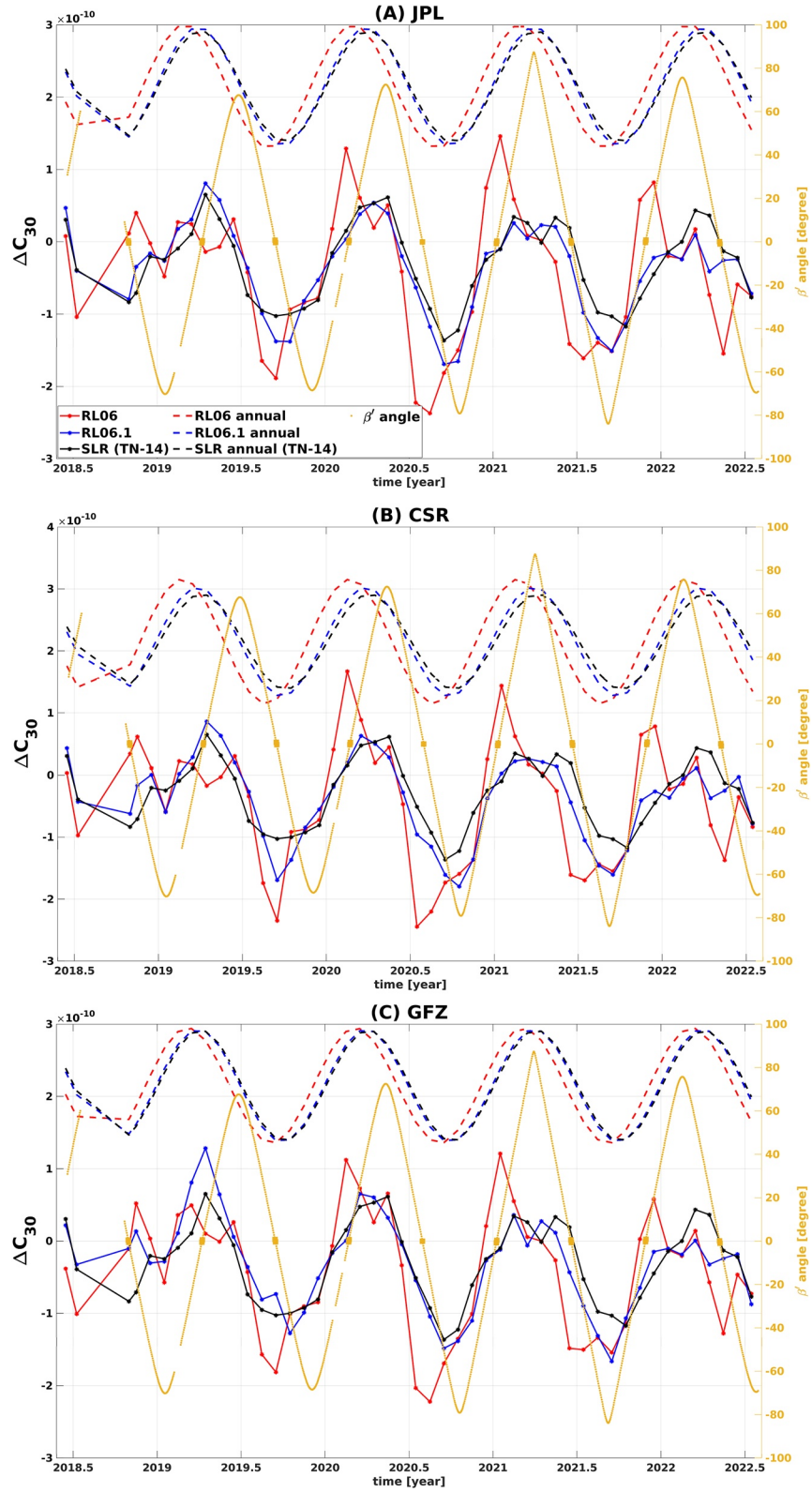

Figure 3. Impact of ACH on $\overline{C}_{30}$. Comparison of the $\Delta\overline{C}_{30}$ geopotential spherical harmonic coefficient from GRACE-FO (a) JPL, (b) CSR and (c) GFZ RL06 (solid red line) and RL06.1 (solid blue line) and Satellite Laser Ranging (solid black line) as provided in the currently used version 2 of TN-14. The GRACE-FO β' angle (yellow) is also shown. Annual cycle of the $\overline{C}_{30}$ timeseries, shown by dashed lines, demonstrates the positive impact of ACH on recovery of the seasonal variability in $\overline{C}_{30}$, particularly in terms of its phase.

Table 1
Annual Amplitude, Annual Phase (in Degrees) and Trend of $\Delta\overline{C}_{30}$ From GRACE-FO and Satellite Laser Ranging (SLR) Computed for the Period of June 2018 to July 2022

		RL06	RL06.1	SLR (TN-14)	SLR (updated TN-14)
JPL	Annual amplitude	8.54E−11	8.18E−11	7.68E−11	7.88E−11
	Annual phase (deg)	259.21	288.40	292.53	289.61
	Trend	−1.13E−11	−1.41E−11	−3.79E−12	−1.19E−11
CSR	Annual amplitude	1.01E−10	8.80E−11	7.68E−11	7.88E−11
	Annual phase (deg)	250.74	284.45	292.53	289.61
	Trend	−1.27E−11	−1.50E−11	−3.79E−12	−1.19E−11
GFZ	Annual amplitude	7.99E−11	7.81E−11	7.68E−11	7.88E−11
	Annual phase (deg)	265.21	288.48	292.53	289.61
	Trend	−9.33E−12	−1.60E−11	−3.79E−12	−1.19E−11

Note. "SLR (TN-14)" denotes the current version 2 of TN-14 and "SLR (updated TN-14)" denotes a new test release for version 3 of TN-14 providing SLR $\overline{C}_{30}$ estimates computed by updating the time-variable gravity used in SLR processing. $\Delta\overline{C}_{30}$ is computed from the difference between GRACE-FO and GGM05C $\overline{C}_{30}$.

satellites. To that end, we performed spectral analysis of the GRACE-FO SDS L2 solutions from RL06 and RL06.1 to SH degree 96. Our study period consists of 48 monthly L2 solutions (from June 2018 to July 2022). The following spectral analyses were performed based on the average of the 48 monthly solutions. The anomalous SH coefficients of degree l and order m, $\{\Delta\overline{C}_{lm}, \Delta\overline{S}_{lm}\}$, representing time-variable gravity were obtained by removing the static gravity signal based on the background model GGM05C.

We computed the degree amplitude σ_l and order amplitude σ_m of L2 data using

$$\sigma_l = \sqrt{\sum_{m=0}^{l} \Delta\overline{C}_{lm}^2 + \Delta\overline{S}_{lm}^2}; \quad l = 2, 3, \ldots, L_{\max} \tag{1}$$

$$\sigma_m = \sqrt{\sum_{l=m}^{L_{\max}} \Delta\overline{C}_{lm}^2 + \Delta\overline{S}_{lm}^2}; \quad m = 0, 1, 2, \ldots, L_{\max} \tag{2}$$

where $L_{\max}$ is the maximum degree of L2 data, which is 96 in our case. The degree and order amplitudes indicate the power of the time-variable gravity spectrum associated with SH coefficients of the same degree and order, respectively. We note that while the degree amplitude is related to the energy of gravity signal (Kaula, 1966), the order amplitude does not carry any physical meaning. Despite that, we found the order amplitude analysis a handy spectral analysis tool for our purpose (see below).

Degree amplitudes of JPL, CSR, and GFZ L2 solutions from RL06 and RL06.1 as well as their difference, are shown in Figures 5a–5c, respectively. The degree amplitudes show a decaying behavior from degree 2 to ∼40, and then start to increase. This indicates that the spectrum of the L2 data is dominated by time-variable gravity signals from degree 2 to ∼40, and by noise from degree ∼40 to 96. We see that the degree amplitude curves of RL06 and RL06.1 start to deviate from each other, starting at degree ∼40, with that of RL06.1 showing a smaller magnitude, consistently for all the SDS solutions. This indicates that noise is reduced in RL06.1 for all L2 solutions from JPL, CSR and GFZ. Among the three SDS solutions, the GFZ data shows the largest noise in RL06 and RL06.1 and also the largest update (represented by black line) due to ACH. Examining the degree amplitudes of individual monthly L2 data over the study period indicates a β' angle-dependent behavior, showing larger noise reduction for months with near-zero GRACE-FO β' angle (not shown).

Figures 5d–5f show the order amplitudes of JPL, CSR and GFZ L2 data from RL06 and RL06.1 as well as their difference, respectively. The notable peaks in the order amplitudes of RL06 and RL06.1 data are associated with the resonant orders of GRACE-FO satellites being ∼15, 30, 45, 60, 75, and 90 (Kaula, 1966). These are multiple integers of the basic resonant order (i.e., ∼15 or 16), approximately equal to the number of revolutions of GRACE-FO satellites per day. The order amplitudes of RL06.1 are particularly smaller than those of RL06 at the

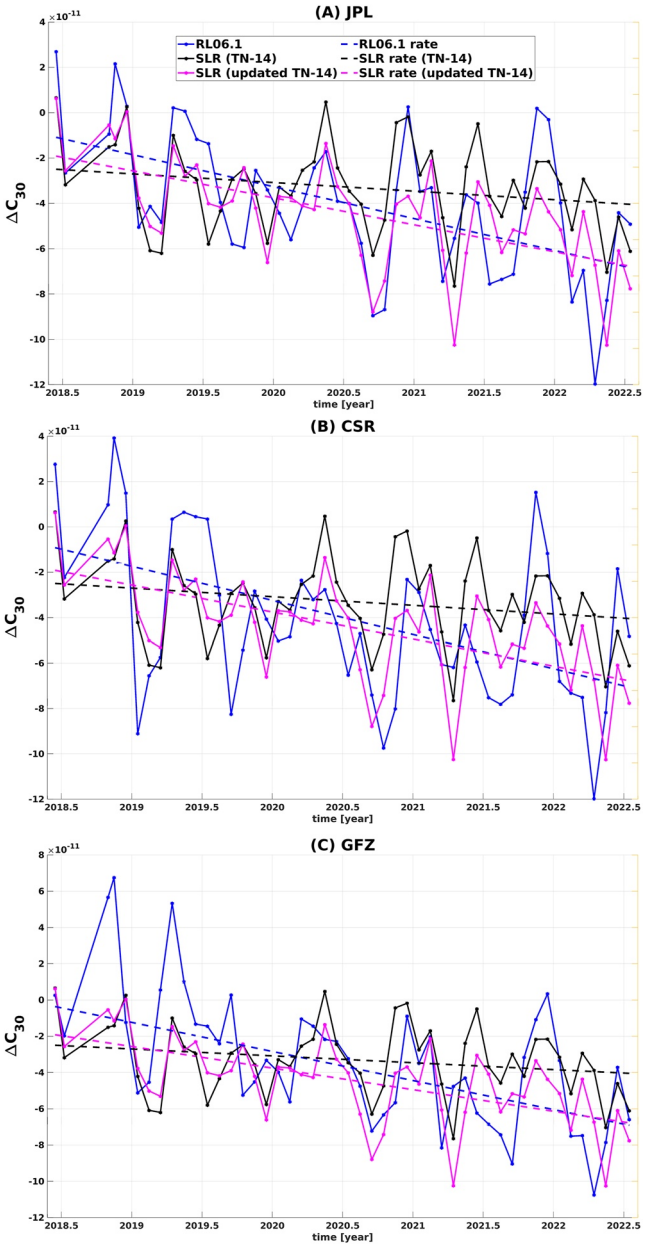

Figure 4. Impact of ACH on $\overline{C}_{30}$. Comparison of deseasonalized timeseries of the geopotential spherical harmonic coefficient $\Delta\overline{C}_{30}$ from GRACE-FO (a) JPL, (b) CSR and (c) GFZ RL06.1 (solid blue line) and Satellite Laser Ranging (SLR) (solid black line) as provided in the currently used version 2 of TN-14. The deseasonalized SLR $\Delta\overline{C}_{30}$ timeseries from a new test release of version 3 of TN-14 (solid magenta line) is also shown. Dashed lines show the linear trend of the $\Delta\overline{C}_{30}$ timeseries. The updated SLR $\overline{C}_{30}$ better fits the GRACE-FO value in terms of interannual variability and linear trend. The new SLR $\overline{C}_{30}$ is computed by updating the background time-variable gravity model used in SLR data processing.

resonant orders. This shows that the largest improvement by ACH happens for the geopotential SH coefficients associated with resonant orders (see black lines) resulting from the specific orbit sampling of the Earth gravity field by GRACE-FO satellites.

JPL and GFZ L2 data also show notable improvement for SH orders next to the resonant orders, while CSR data only show a large improvement at the resonant orders. As can be inferred from Equation 2, order amplitude for a SH order m involves all the SH coefficients from degree m to $L_{\max} = 96$. The high degree coefficients above, for example, 60, are highly contaminated with noise. Thus, the high degree coefficients could significantly affect the order amplitude values. We truncated the L2 data at SH degree and order 60 and recomputed the order amplitudes. The results shown in Figures 5g–5i clearly illustrate the distinct improvement at resonant orders for all the SDS solutions. A comparison of Figures 5g–5i indicates that GFZ RL06.1 shows the largest improvement at resonant orders compared to other SDS solutions. Also, CSR L2 data does not show a clear peak at the basic resonant order ~15, which could be related to the so-called 2-step procedure (i.e., separate estimation of arc parameters and geopotential coefficients) applied in producing the CSR L2 solutions.

3.3. Noise Reduction in GRACE-FO Mass Change Estimates Over Oceans From RL06.1

Surface mass change estimated from GRACE and GRACE-FO monthly L2 data is frequently used to study various geophysical processes in the Earth system. We examined the noise of mass change data from GRACE-FO RL06 and RL06.1 solutions to quantify the improvement by the new accelerometer transplant data ACH. To that end, we used the GRACE-FO L2 data to a maximum degree of 60, replaced the $\overline{C}_{20}$ and $\overline{C}_{30}$ coefficients with the SLR-derived values from TN-14, added degree-1 SH coefficients from TN-13, and applied a Gaussian filter with a 300 km radius to reduce the noise (Jekeli, 1981). We then computed surface mass change in terms of equivalent water height on the reference ellipsoid from filtered L2 data on a global grid with 0.5° resolution (Ghobadi-Far, Šprlák, & Han, 2019). Next, we removed the climatology signal (by fitting and removing a model for linear trend plus semi-annual and annual variability) as well as interannual variability from mass change timeseries at each grid cell (e.g., Chen et al., 2021). The interannual variability was removed by applying a high-pass filter to the residual timeseries (obtained after subtracting the climatology) with a cut-off period of 1 year. Finally, we considered the RMS of residual mass change timeseries for each grid cell over the oceans as an estimate of noise in the GRACE-FO mass change data (e.g., Chen et al., 2021; Kvas et al., 2019).

Figure 6 shows the spatial maps of noise estimates of GRACE-FO mass change over oceans from RL06 and RL06.1 for JPL (6A and B), CSR (6C and D) and GFZ (6E and F) solutions. The results show a clear noise reduction by RL06.1 that is more evident for JPL and GFZ solutions due to their higher noise level and, thus, higher noise reduction. We computed minimum, maximum and mean noise estimates over open oceans considering a 300 km buffer from land to reduce the leakage of strong land signals into the oceans. The results reported in Table 2 show that RL06.1 improves upon RL06 in terms of all statistics. For example, mean of noise estimates over the open oceans from JPL, CSR and GFZ solutions is reduced from 3.24 to 3.01 cm, from 2.54 to 2.4 cm, and from 3.98 to 3.75 cm, respectively. Figures 7a–7c show the spatial maps of improvement in percentage by RL06.1 for JPL, CSR and GFZ data, respectively. We see up to a 20% reduction in noise

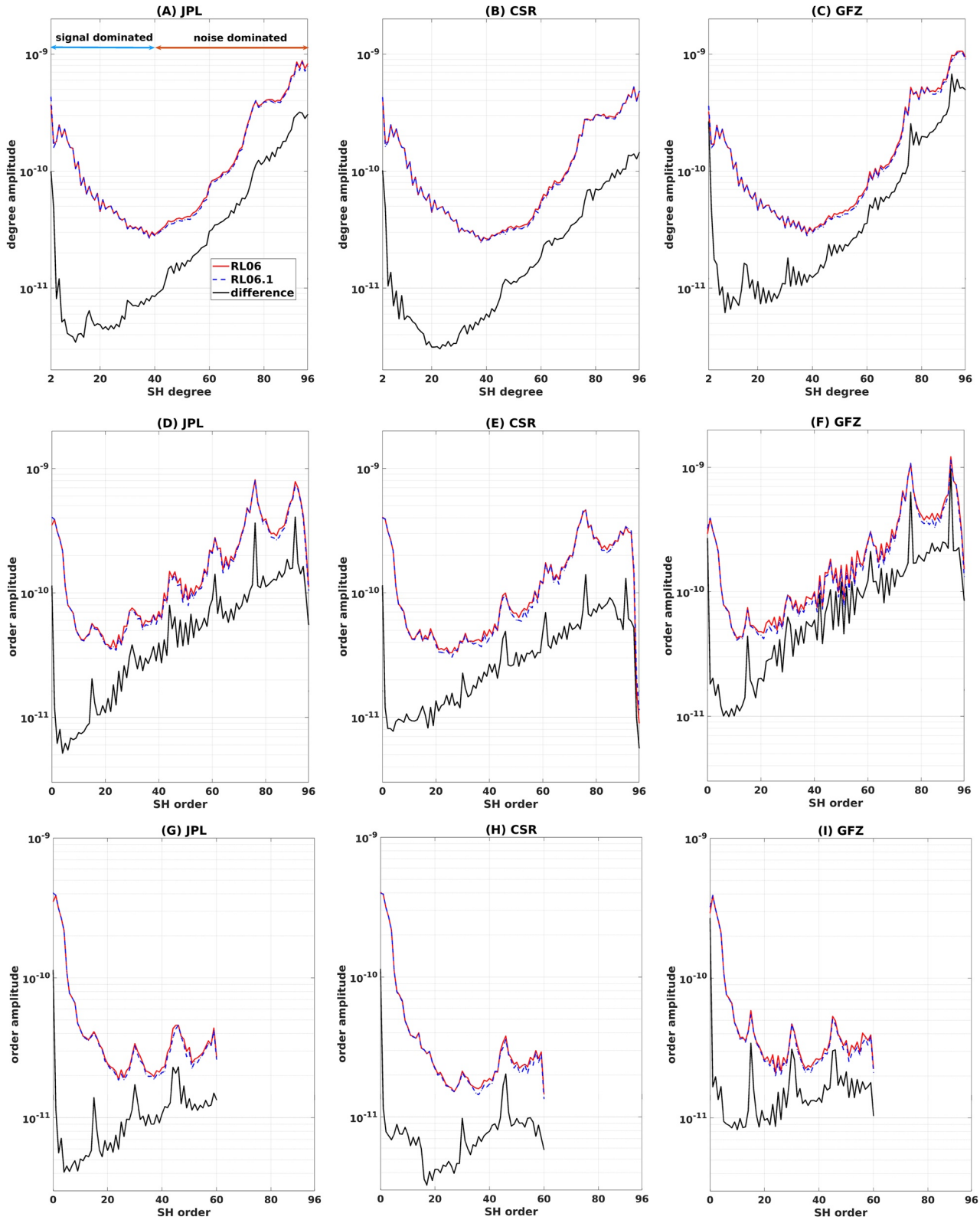

Figure 5. Spectral analysis of GRACE-FO L2 data. Degree amplitudes of GRACE-FO (a) JPL, (b) CSR, and (c) GFZ RL06 (red) and RL06.1 (blue) as well as their difference (black) computed from L2 spherical harmonic (SH) coefficients to degree 96. Order amplitudes of GRACE-FO RL06 (red) and RL06.1 (blue) as well as their difference (black) computed from L2 SH coefficients to degree 96 in the case of (d) JPL, (e) CSR and (f) GFZ data, as well as computed from L2 SH coefficients truncated to degree 60 in the case of (g) JPL, (h) CSR, and (i) GFZ data. The largest improvement by ACH occurs for the SH coefficients associated with resonant orders (i.e., 15, 30, 45, etc.).

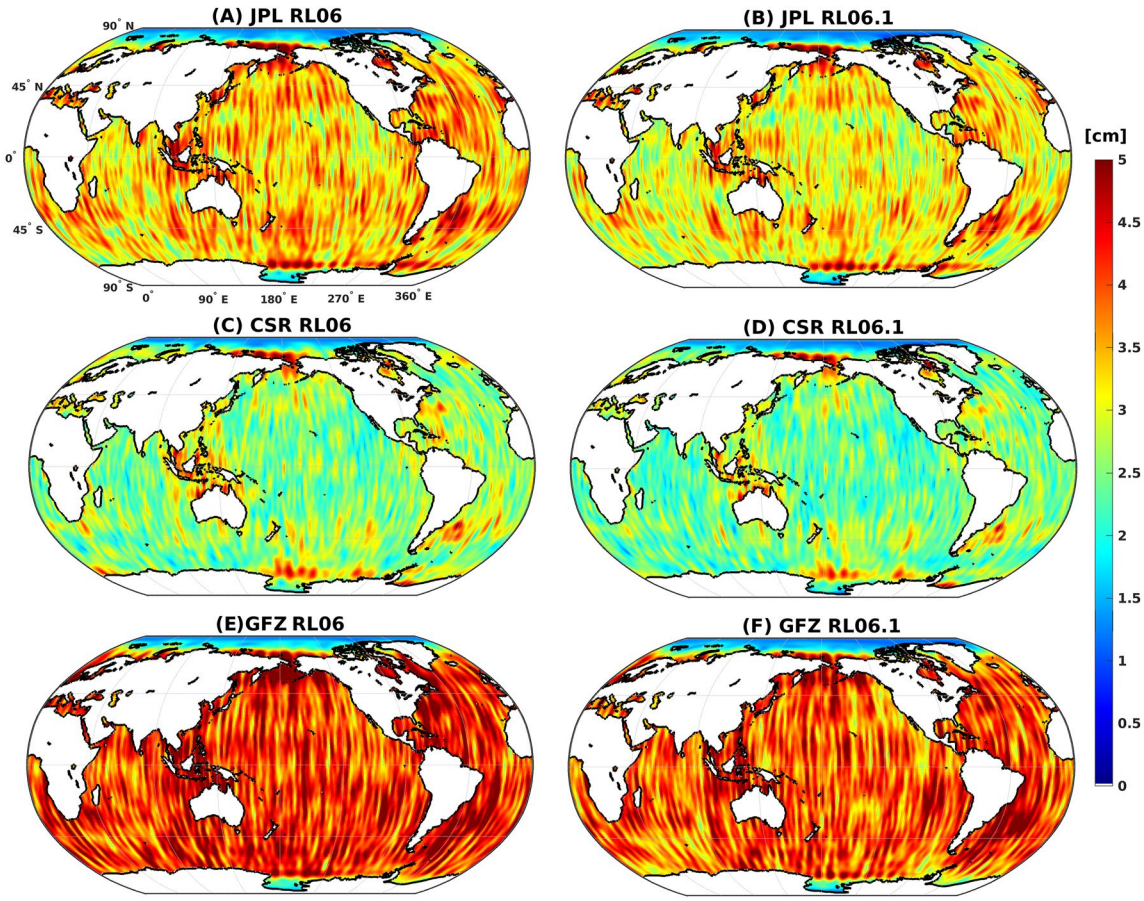

Figure 6. Noise assessment of GRACE-FO mass change data in the space domain over oceans. Noise estimates of mass change data over oceans from RL06 and RL06.1 computed for (a and b) CSR, (c and d) JPL, and (e and f) GFZ solutions. Mass change is estimated from L2 data after applying a Gaussian filter with 300 km radius.

manifested as north-south stripes in all the SDS solutions. The average improvement along the parallels with constant latitudes is provided in Figure 7d, and it shows ∼5% to 10% noise reduction. JPL data shows the largest improvement by RL06.1 from −50° to +50° latitude.

We also examined the temporal evolution of noise in GRACE-FO mass change by computing the RMS of residuals over the open oceans for each monthly data. The timeseries of monthly noise estimates for JPL, CSR and GFZ data are shown in Figures 8a–8c, respectively. Timeseries of the GRACE-FO β' angle is also shown. The noise estimates from RL06.1 are smaller than those from RL06 for almost all the months, indicating the positive impact of ACH on GRACE-FO L2 data. The largest noise in RL06 solutions and, consequently, the largest noise reduction by RL06.1 happens for months with near-zero β' angle. The increased noise in GRACE-FO monthly data starting in late 2021 is due to increasing solar activity during this period, which is caused by an upramping of the nearly periodic 11-year solar magnetic activity cycle. This is expected to last over the next few years (Landerer et al., 2022), making an improved accelerometer transplant even more important.

To make sure the above results are not affected by the relatively weak filter applied (i.e., 300 km radius Gaussian filter) to L2 data, we repeated the GRACE-FO noise estimates analysis but this time after applying the decorrelation filter of Swenson and Wahr (2006) plus a Gaussian filter with 300 km radius. The decorrelation filter is more effective in reducing the north-south stripes in GRACE mass change fields. The results of the new analyses are shown in Figures 9–11. Statistics of the spatial maps of noise estimates shown in Figure 9 indicate the noise reduction for all the SDS solutions (see Table 2). We see the largest improvement by RL06.1 in the space domain for GFZ data (see Figures 9e and 9f, and also Figure 10c). The new accelerometer transplant data ACH leads to an improvement of ∼5% in terms of the average noise estimates over the parallels (Figure 10d). The timeseries of monthly noise estimates again show a β' angle-dependent behavior, with the largest improvement

Table 2
Minimum, Maximum, and Mean of Noise Estimates in cm of Equivalent Water Height Over Open Oceans (Considering a 300 km Buffer From Land) Computed From RL06 and RL06.1 of GRACE-FO Science Data System Solutions (See Figures 6 and 9)

			RL06	RL06.1	Improvement %
G300 km	JPL	Min.	1.16	1.11	4
		Max.	6.75	5.73	15
		Mean	3.24	3.01	7
	CSR	Min.	1.16	1.08	7
		Max.	5.67	5.39	5
		Mean	2.54	2.40	6
	GFZ	Min.	1.17	1.10	6
		Max.	7.07	6.89	3
		Mean	3.98	3.75	6
DC + G300 km	JPL	Min.	0.37	0.38	−3
		Max.	2.59	2.44	6
		Mean	1.10	1.06	4
	CSR	Min.	0.34	0.39	−15
		Max.	2.52	2.55	−1
		Mean	1.02	0.98	4
	GFZ	Min.	0.43	0.42	2
		Max.	2.83	2.54	10
		Mean	1.20	1.12	7

Note. Noise estimates are computed after applying two filtering methods to the L2 data: (a) A Gaussian filter with 300 km radius (G300 km) and (b) the Decorrelation (DC) filter of Swenson and Wahr (2006) plus a Gaussian filter with 300 km radius.

happening for GFZ data (Figure 11). Overall, the results presented in Section 3.3 demonstrate the improvement in the quality of mass change data from all GRACE-FO SDS RL06.1 solutions caused by the high-quality non-gravitational accelerations provided in ACH.

3.4. Quantification of the Impact of ACH on Greenland and Antarctic Ice-Sheet Mass Change From GRACE-FO L2 Data and Comparison With Altimetry

We quantified the impact of ACH on ice-sheet mass change in Greenland and Antarctica during the GRACE-FO period by comparing the RL06 and RL06.1 solutions. To that end, we used the mass change estimation method of tailored sensitivity kernels, which defines sensitivity kernels in a formal optimization by minimizing the sum of both the GRACE error effect and leakage error (Döhne et al., 2023; Groh & Horwath, 2021). The sensitivity kernels are then applied to the L2 SH coefficients in order to estimate integrated mass changes over the target regions. We used SH coefficients up to degree 90, added degree-1 coefficients derived from a combination of the monthly solutions and assumptions on ocean mass redistribution (Bergmann-Wolf et al., 2014; Sun et al., 2016; Swenson et al., 2008), and replaced the $\overline{C}_{20}$ and $\overline{C}_{30}$ coefficients with values from the TN-14 (Loomis et al., 2020). To account for glacial isostatic adjustment (GIA), we removed linear trends given by models from Ivins et al. (2013) and Caron et al. (2018) for Antarctica and Greenland, respectively. We then computed linear trends and noise levels of the resulting timeseries of mass changes. The trends were estimated by fitting a quadratic polynomial together with annual and semi-annual sinusoids to the timeseries. Uncertainty assessment of the trends includes the formal uncertainty of the fit, uncertainties associated with leakage, the GIA correction, and the degree-1 and $\overline{C}_{20}$ coefficients. We refer to Groh and Horwath (2021) for details of the uncertainty assessment. Quantification of the noise level was carried out based on filtering the residuals of the model fit with a high-pass filter based on a Gaussian average and using the scaled standard deviation of the filtered timeseries as an estimate of the noise level (see Groh et al. (2019) for more details).

Trend and noise level estimates for both ice-sheets are shown in Figure 12. For the Antarctic Ice-Sheet, the trend estimates from SDS RL06 solutions are −76 Gt/yr and −77 Gt/yr for JPL and CSR, respectively and −95 Gt/yr for GFZ. The RL06.1 trends are ∼20–25 Gt/year less negative than the RL06 trends for all three SDS solutions. Updating the $\overline{C}_{20}$ and $\overline{C}_{30}$ coefficients based on the new test release of version 3 of TN-14 results in a 9 Gt/year less negative trend for all three SDS solutions compared to using the current version 2 of the TN-14. In the case of the Greenland Ice-Sheet, trend differences between RL06 and RL06.1 are much smaller and range from −1 to +3 Gt/yr. The impact of switching to the updated TN-14 is an 11 Gt/year more negative trend for all three SDS solutions in this case. Note that the differences in trend estimates for Greenland and Antarctica from RL06 and RL06.1 and from switching to the updated TN-14 are smaller than the estimated trend uncertainties (i.e., 46 to 48 Gt/yr for Antarctica and 16 Gt/yr for Greenland).

We see a significant noise reduction in RL06.1 estimates of ice-sheet mass change (Figure 12b). In the case of CSR and JPL RL06.1 solutions, the noise reduction is as large as 30 Gt. This number is ∼18 Gt in the case of GFZ RL06.1 data. Examining the mass change timeseries of the Antarctic Ice-Sheet clearly demonstrates the noise reduction by RL06.1 for multiple months, including September 2019 and January 2021 (see Figure S4 in Supporting Information S1). Moreover, Figure S4 in Supporting Information S1 shows that, due to its β'-dependent behavior, the update by ACH mainly affects the semi-annual and, to a lesser extent, annual variability in the ice sheet mass change timeseries, in particular in the case of Antarctica. We similarly observed a significant reduction of noise levels for the Greenland Ice-Sheet by switching from RL06 to RL06.1. JPL, CSR, and GFZ solutions show noise reduction by 4, 8, and 8 Gt in this case, respectively. We also quantified the change

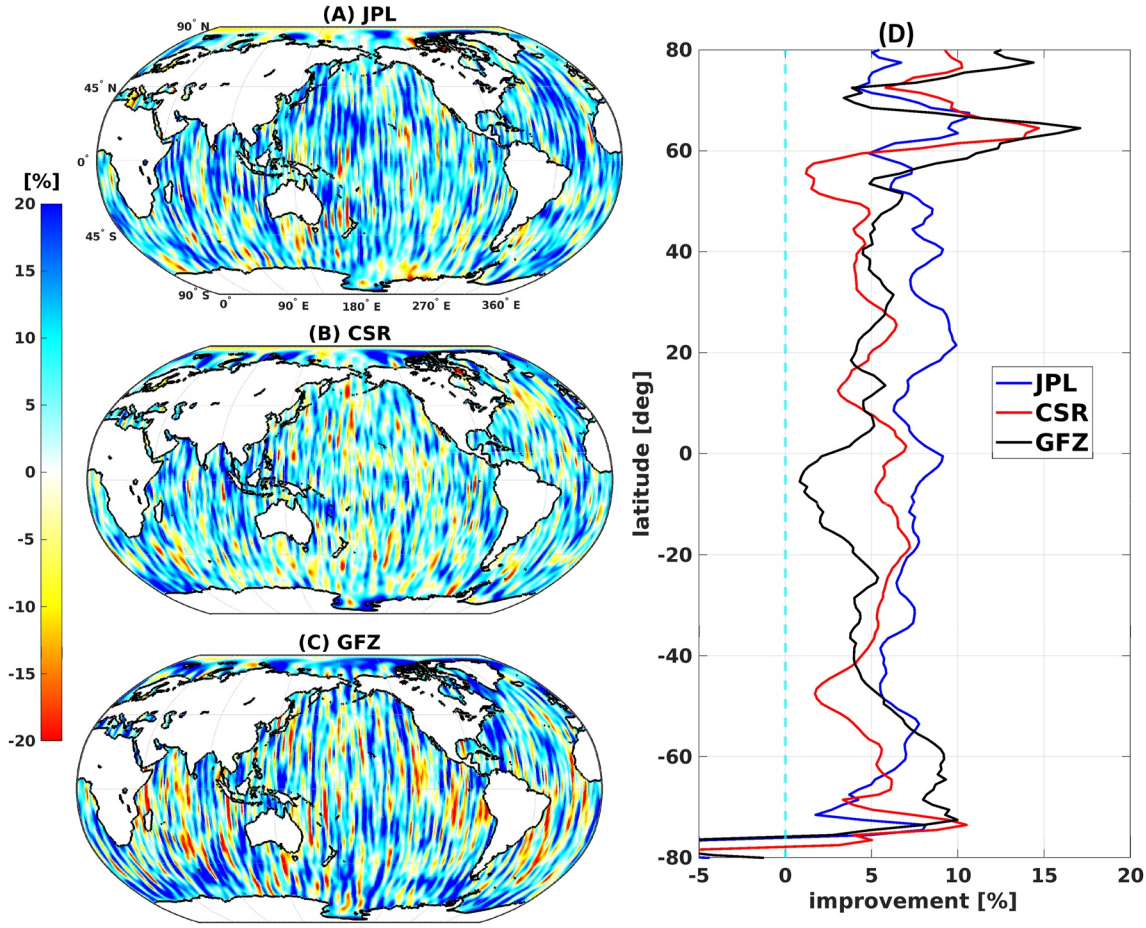

Figure 7. Noise assessment of GRACE-FO mass change data in the space domain. Spatial maps of relative noise reduction in percentage from RL06 to RL06.1 in the case of (a) JPL, (b) CSR, and (c) GFZ data. (d) Average improvement in percentage over parallels with constant latitudes is also shown. Mass change is estimated from L2 data after applying a Gaussian filter with 300 km radius.

in trend and noise level by RL06.1 for the individual ice drainage basins defined by Zwally et al. (2012) in Antarctica, confirming a similar noise reduction for most basins (see Figures S5 and S6 of Supporting Information S1).

For a tentative validation of the ACH impact on GRACE-FO L2 data, we compared GRACE-FO SDS estimates of ice-sheet mass change to independent results based on data from the CryoSat-2 and ICESat-2 satellite altimetry missions (updated from Helm et al., 2014). For this comparison, we defined a benchmark region within the East Antarctic Ice-Sheet (Figure S7 in Supporting Information S1). This region is the upper part of the East Antarctic Plateau with >3,500 m surface elevation given by REMA DEM data (Howat et al., 2019). We use this region for evaluation because we expect the mass change to be very small due to arid conditions. The annual average surface mass balance over the benchmark region amounts to 34 mm/yr in terms of equivalent water height during the time period 1979–2021 (updated according to van Wessem et al. (2018)). At the same time, errors of the altimetry results (which depend on topographic roughness) and of the GRACE-FO results (which include leakage errors and hence depend on regional mass change amplitudes) are expected to be small in this benchmark region.

We used surface elevation products derived from the CryoSat-2 and ICESat-2 altimetry data, which fully cover this region due to their orbit design. The volume changes were converted to mass changes with a time-independent firn density using the empirical Equation 2 in Ligtenberg et al. (2011). The mean firn density in our benchmark region is 331 kg/m³. We disregard elevation changes due to ice-flow dynamics as we assume they have no major impact on the mass balance in this region (Martín-Español et al., 2017). We then compared (a) mean rates of the GRACE-FO mass change and altimetry data, and (b) RMS difference between detrended GRACE-FO and altimetry mass change timeseries. GRACE-FO and altimetry timeseries are shown in Figure S7 of Supporting Information S1. We assessed the uncertainty of the altimetry-based mass change rates similar to Willen et al. (2022).

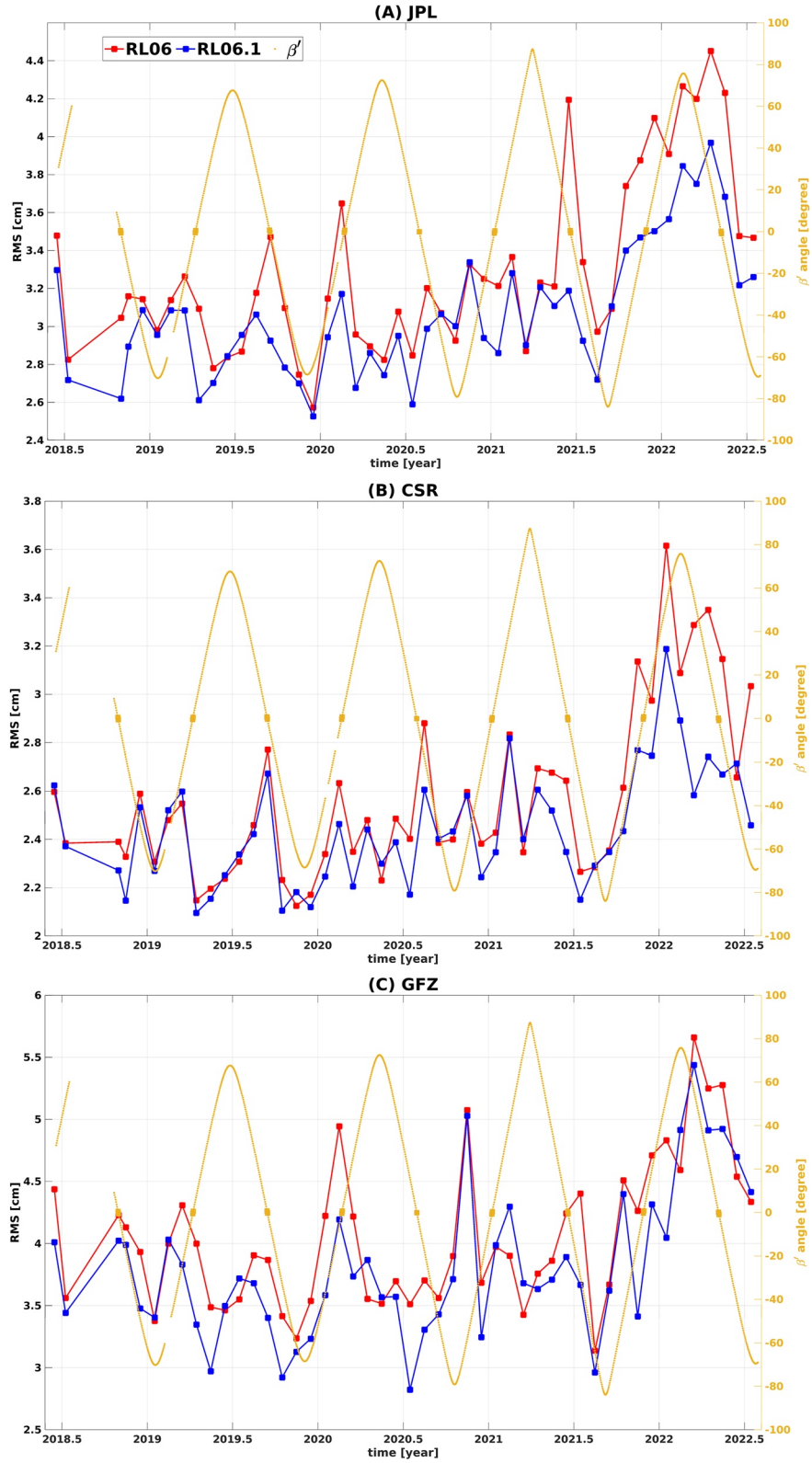

Figure 8. Noise assessment of GRACE-FO mass change data over oceans in the time domain. Timeseries of noise estimates of monthly mass change over open oceans from RL06 (red) and RL06.1 (blue) for (a) JPL, (b) CSR, and (c) GFZ data. Timeseries of GRACE-FO β' angle (yellow) is also shown. The largest noise reduction in RL06.1 happens for months with near-zero β' angle. Mass change is estimated from L2 data after applying a Gaussian filter with 300 km radius. Note the different y-axes used for (a–c).

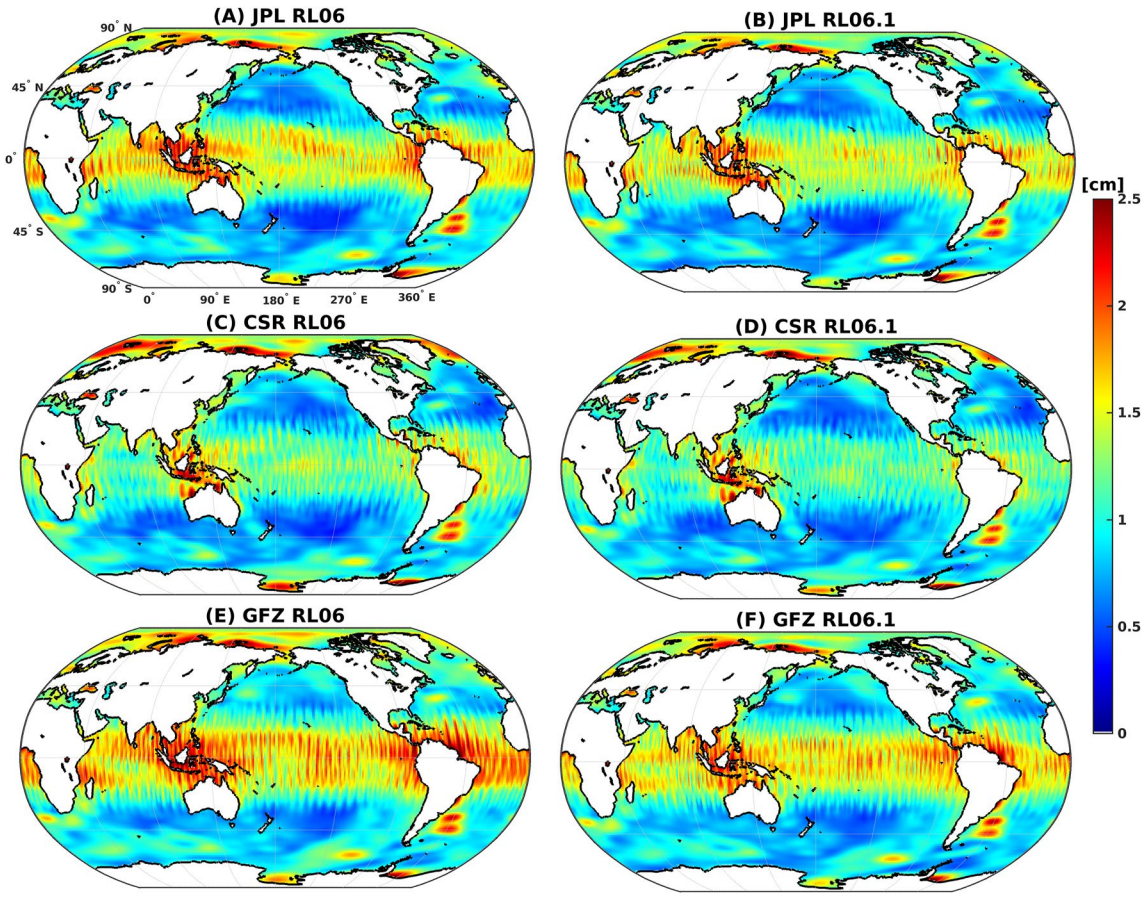

Figure 9. Same as Figure 6, but based on mass change data computed from L2 solutions after applying the decorrelation filter of Swenson and Wahr (2006) plus a Gaussian filter with 300 km radius.

We propagated the error-covariance information derived from a CryoSat-2 trend ensemble to the basin mean trend. Currently, there is no rigorous uncertainty characterization of ICESat-2 data available. As a conservative uncertainty estimate, we consider the empirically characterized CryoSat-2 uncertainty as an upper limit for the ICESat-2 data. As a rough uncertainty assessment for the firn density, we assumed that its uncertainty is 10% of its magnitude, that is, 33 kg/m³. Additionally, we included the GRACE-FO ITSG-Grace2018 solutions (Kvas et al., 2019) in this analysis. Ditmar (2022) found that ITSG-Grace2018 solutions show the lowest noise level among available GRACE products. As such, we wanted to see if the GRACE-FO SDS solutions from RL06.1 are closer to ITSG-Grace2018 when compared to altimetry data.

For each of the three GRACE-FO SDS variants, GFZ and CSR show the smallest and highest mean rates, respectively (see Figure 13a). The GFZ RL06 mean rate, -3.4 ± 4.2 mm/yr in terms of equivalent water height, deviates the most from the altimetry mean rates. The CryoSat-2 and ICESat-2 mean rates are 1.3 ± 2.8 and 5.5 ± 2.8 mm/yr, respectively. In the case of ICESat-2 comparison, the mean rate derived from CSR RL06.1 based on the updated TN-14 shows the least deviation (5.7 ± 3.9 mm/yr). The RMS difference of the timeseries from RL06.1 is significantly smaller than that from RL06 (Figure 13b). We note that RMS difference calculated with ICESat-2 data is slightly smaller than that with CryoSat-2. The lowest RMS difference value of 9.3 mm equivalent water height arises between CSR RL06.1 (based on updated TN-14) and ICESat-2. In general, we see that the mean of the RL06.1 SDS and ITSG-GRACE-2018 solutions show a similar agreement to the altimetry data. Finally, the analyses presented in this section are further indications of the effectiveness of the ACH data product.

4. Impact of ACH on GRACE-FO Mascon Data

Mascon solutions and L3 mass change data products from GRACE and GRACE-FO provide easy-to-use data sets for Earth system mass change monitoring without requiring post-processing. We investigated the impact of the

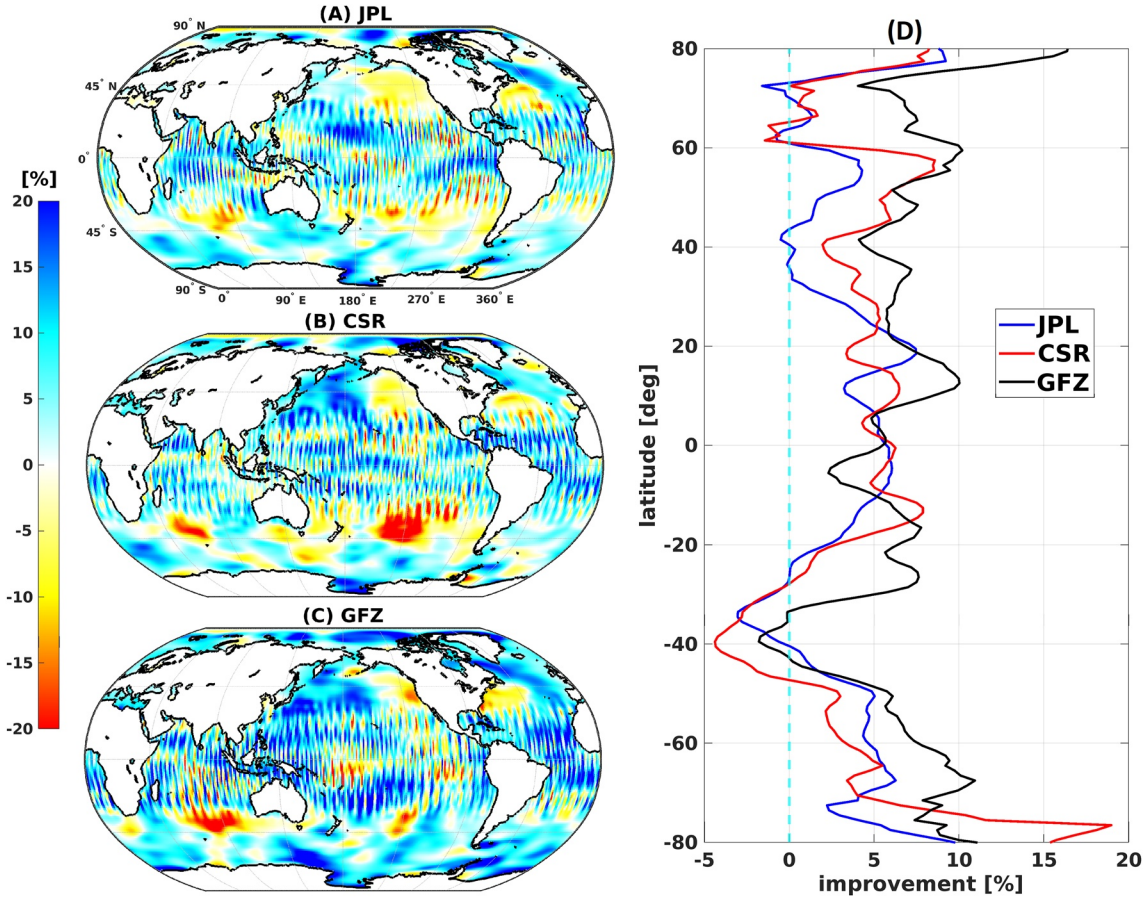

Figure 10. Same as Figure 7, but based on mass change data computed from L2 solutions after applying the decorrelation filter of Swenson and Wahr (2006) plus a Gaussian filter with 300 km radius.

new accelerometer transplant data ACH on the GRACE-FO mascon solutions released by NASA JPL (Watkins et al., 2015) and NASA GSFC (Loomis, Luthcke, & Sabaka, 2019) and L3 gridded mass change data from GFZ (see http://gravis.gfz-potsdam.de/home). GRACE-FO mascon solutions from the Center for Space Research of the University of Texas at Austin (Save et al., 2016) based on ACT and ACH were not available to the public at the time of writing this paper. Figures 14a and 14c show the JPL and GSFC mascon solutions in terms of equivalent water height for January 2019. The change in the mascon solution of this month caused by updating the accelerometer data from ACT to ACH is shown in Figures 14b and 14d in the case of JPL and GSFC data, respectively. The update by ACH causes stripe-like changes in mascon data with a magnitude as large as 1 cm, which amounts to ~5% of the signal. Moreover, in the case of JPL mascon solution, we see a high correlation between the magnitude of the update and the signal; the larger the signal, the larger the update by ACH.

Figures 15a, 15c, and 15e show the trend, annual amplitude and RMS variability of the JPL GRACE-FO mascon solutions computed based on monthly data from June 2018 to July 2022. The impact of the ACH on mass change trends shown in Figure 15b is mainly manifested as north-south stripes with both positive and negative values ranging between ±0.5 cm/yr, indicating that ACH does not cause a significant change on JPL mascon trend over the GRACE-FO period. Inspecting the change in annual amplitude shown in Figure 15d leads to the same conclusion as for the trend. The RMS difference computed from mass change timeseries based on RL06.1 and RL06 shown in Figure 15f indicates values as large as 3 cm in locations where the RMS variability of the mass change signal (Figure 15e) is the largest (e.g., Amazon, Gulf of Carpentaria, Bangladesh, India and Caspian Sea). In general, we conclude that the change in mascon solutions by ACH is within the error budget of GRACE-FO mascon solutions from JPL and GSFC.

Finally, Figure 16 shows similar results as Figure 15, but based on GFZ L3 gridded data products of terrestrial water storage and ice sheet mass change. In the case of ice sheet mass change from GFZ L3 data, in addition

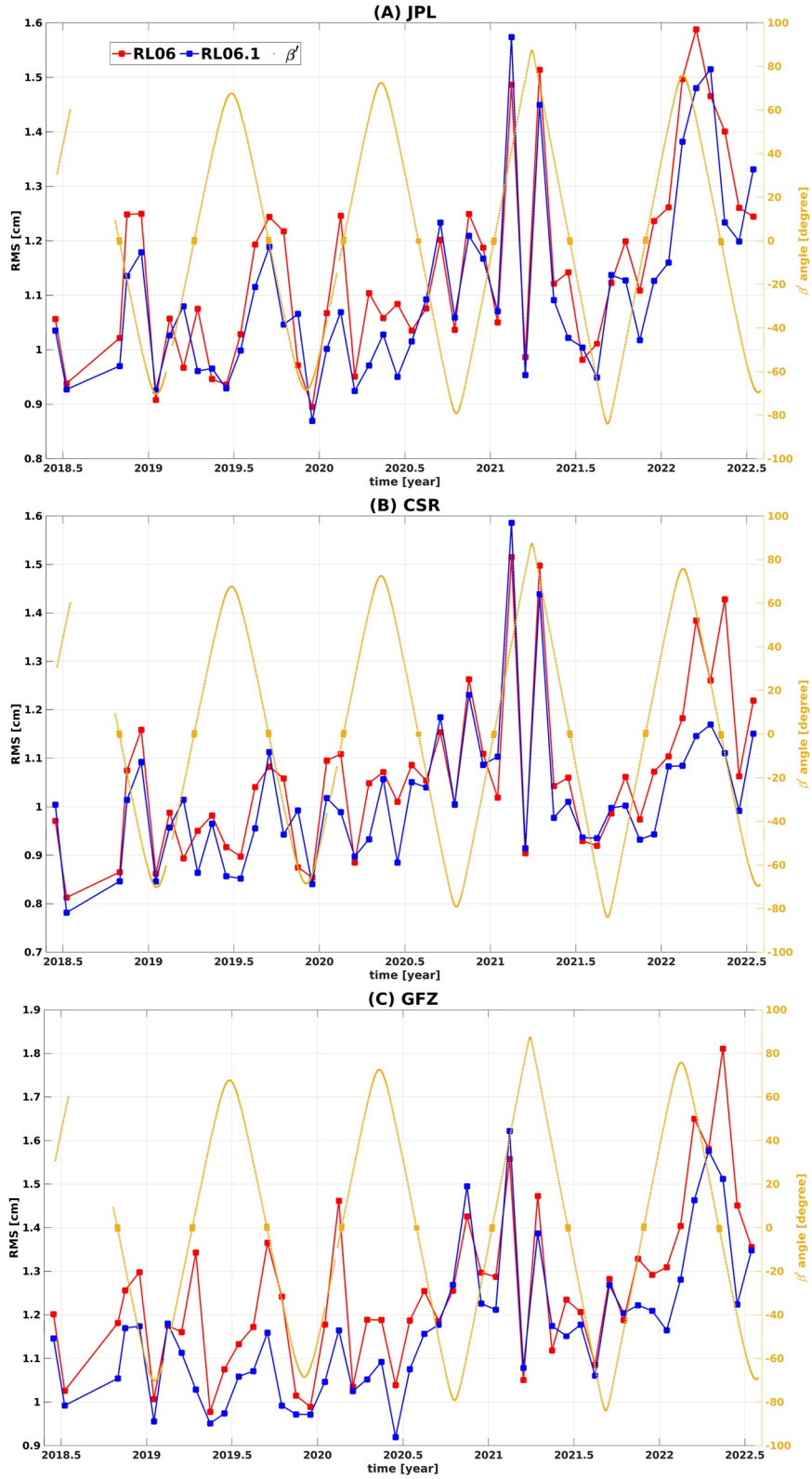

Figure 11. Same as Figure 8, but based on mass change data computed from L2 solutions after applying the decorrelation filter of Swenson and Wahr (2006) plus a Gaussian filter with 300 km radius. Note the different *y*-axes used for (a–c).

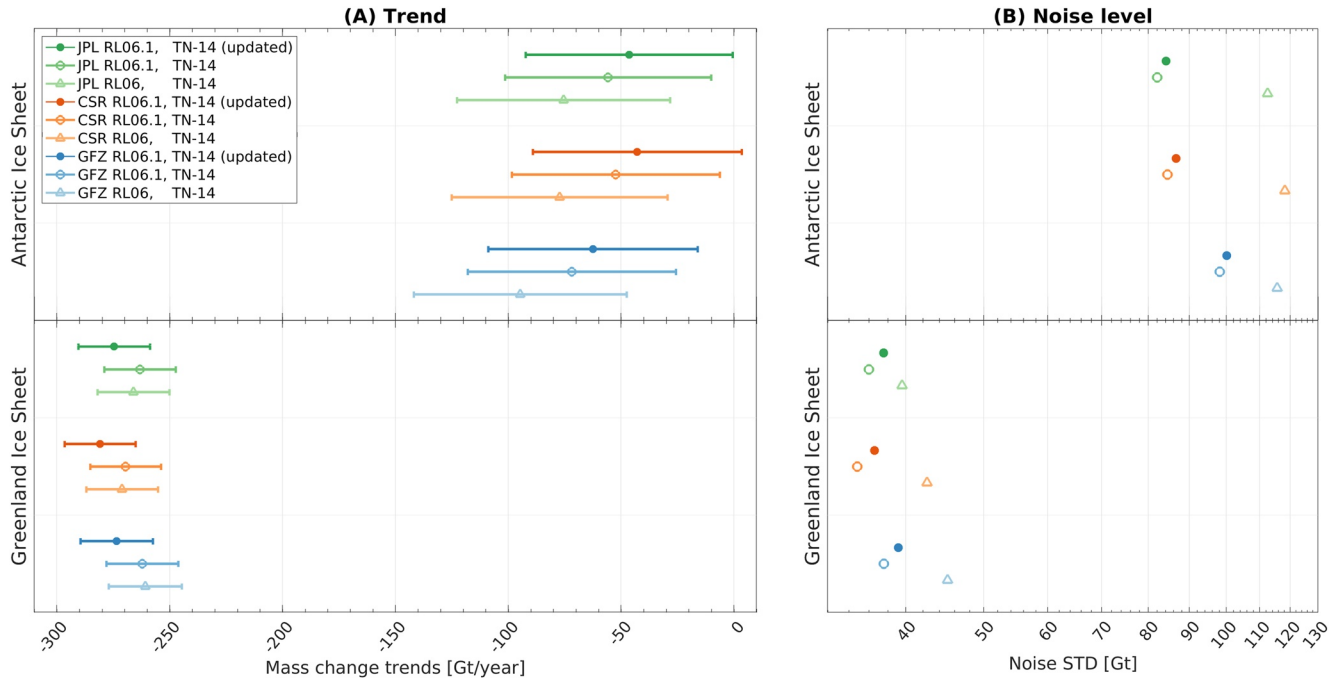

Figure 12. Impact of ACH on ice-sheet mass change estimates. Comparison of (a) trends and (b) noise levels of mass change timeseries of the Antarctic and Greenland Ice-Sheets over the GRACE-FO period computed based on the L2 solutions from RL06 and RL06.1. The effect of the new test release for version 3 of TN-14 is also quantified.

to using RL06.1 in the updated release, the C_{21}, S_{21}, and C_{30} coefficients from GRACE–FO RL06.1 were used. While, for ice sheet mass change from RL06, these coefficients were used from a SLR and GRACE–FO combination (see the changelog file at the GFZ GravIS website). The update by ACH is completely manifested as north-south stripes in the terrestrial water storage changes. In contrast, we see notable changes in the Greenland and Antarctic ice sheet mass change in terms of trend, annual amplitude and RMS variability, which could be partially related to the differences other than using RL06 and RL06.1 in the two estimates as noted above.

5. Conclusions

We examined the impact of the new accelerometer transplant data ACH released by the GRACE-FO SDS on instantaneous inter-satellite ranging data measured along the satellite orbit as well as on monthly snapshots of time-variable gravity and mass change data provided by JPL, CSR and GFZ and GSFC. We showed that inter-satellite ranging residuals from GRACE-FO LRI sensor are modified at low frequencies below 1 mHz. The improvement at low frequencies could lead to more accurate observations of large-scale time-variable gravity signals, such as those from Earth's free oscillations (Ghobadi-Far, Han, et al., 2019) using the along-orbit analysis approach. When mapped into SH domain as in the form of L2 time-variable gravity data, the low-frequency change in inter-satellite ranging residuals leads to improved SH coefficient $\overline{C}_{30}$ as well as coefficients associated with GRACE-FO resonant orders (i.e., 15, 30, 45, etc.). The improvement in $\overline{C}_{30}$ was demonstrated based on a comparison with SLR-derived values provided in the current version 2 of the TN-14. We also presented a test release for version 3 of TN-14, which better fits the GRACE-FO $\overline{C}_{30}$ timeseries at both seasonal (particularly, in terms of phase) and interannual timescales. This demonstrates the high-quality estimates of GRACE-FO $\overline{C}_{30}$ caused by updating the accelerometer transplant data from ACT to ACH.

Our extensive noise analysis of GRACE-FO mass change estimates computed from L2 data over oceans as well as for the Greenland and Antarctic Ice-Sheets proved the significant noise reduction for all RL06.1 solutions from JPL, CSR and GFZ. We showed that the largest noise reduction happens for months with near-zero β' angle. We also examined the impact of ACH on ice-sheet mass change over GRACE-FO period computed from L2 data and concluded that the update from RL06 to RL06.1 has a bigger impact on the mass change estimates of the Antarctic Ice-Sheet than on that of the Greenland Ice-Sheet (on the order of 20–30 Gt/yr compared to −1 to +3 Gt/yr, respectively). The results from altimetry have a similar uncertainty as the results from GRACE-FO. And the

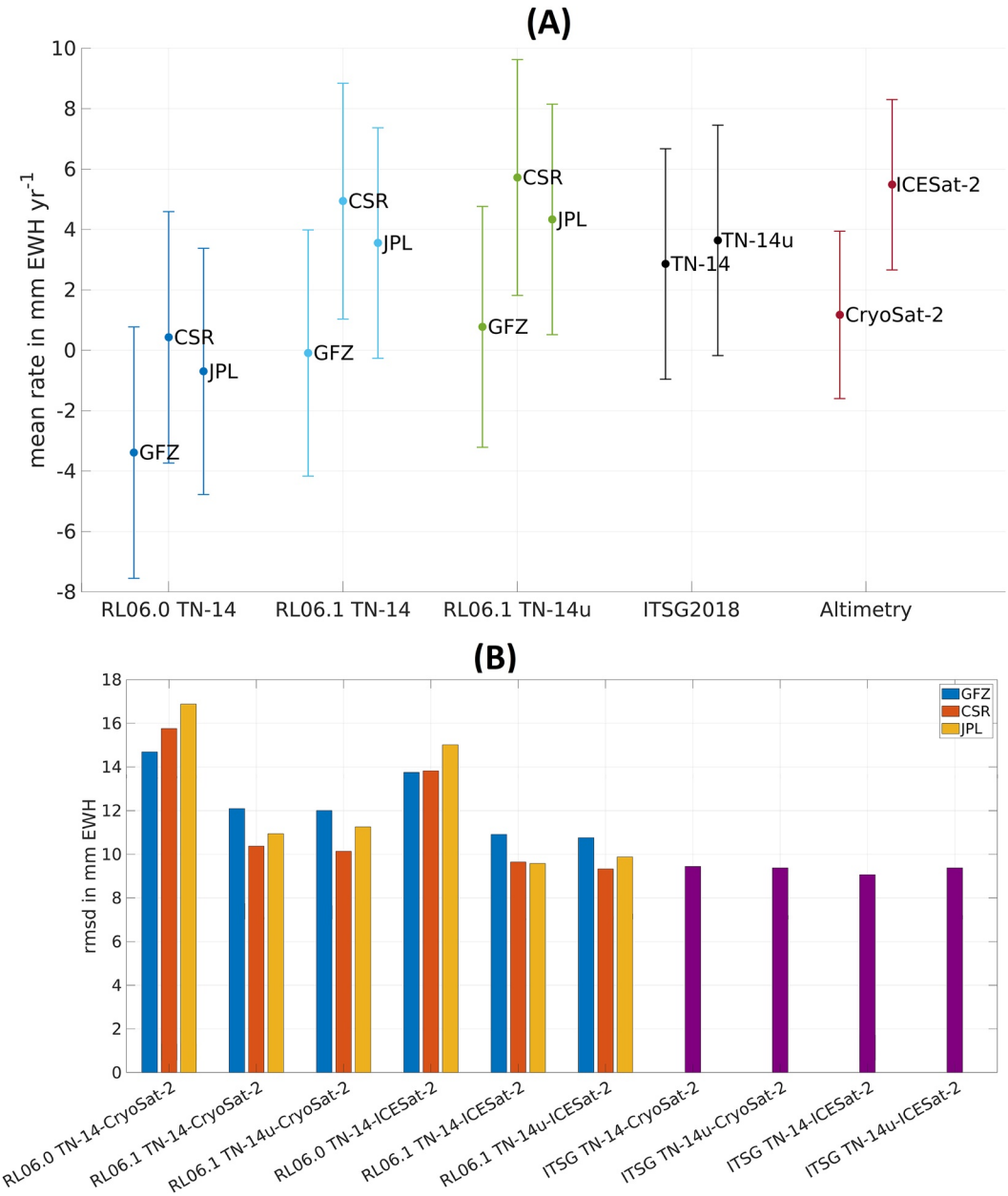

Figure 13. Comparison of ice-sheet mass change estimates based on GRACE-FO and based on satellite altimetry. (a) Comparison of trends in the benchmark region, derived from GRACE-FO Science Data System L2 solutions, ITSG-Grace2018 and satellite altimetry (CryoSat-2 and ICESat-2). See Figure S7 in Supporting Information S1 for the location of the benchmark region. The trends are determined for the time period from October 2018 to March 2022, which is the overlap period of all the data sets. (b) Comparison of the RMS difference between GRACE-FO and altimetry detrended timeseries for the same region and time period (see Figure S7 in Supporting Information S1).

difference between ICESat-2 and CryoSat-2 is of similar magnitude as differences between RL06 and RL06.1, as well as differences between GFZ and CSR or JPL. Therefore, by comparison with altimetry results, we could not conclusively validate an improvement in ice-sheet mass trends through the update from RL06 to RL06.1. However, on average over the three SDS centers and on average over the two altimetry missions, the updated from RL06 to RL06.1 brings the ice mass trend closer to the altimetry result and also closer to the ITSG-Grace2018 solutions, which use their own independent accelerometer transplant method. Assessment of the update by ACH on the mascon solutions from NASA JPL and GSFC showed up to 1 cm changes in terms of equivalent water height manifested mostly as north-south stripes.

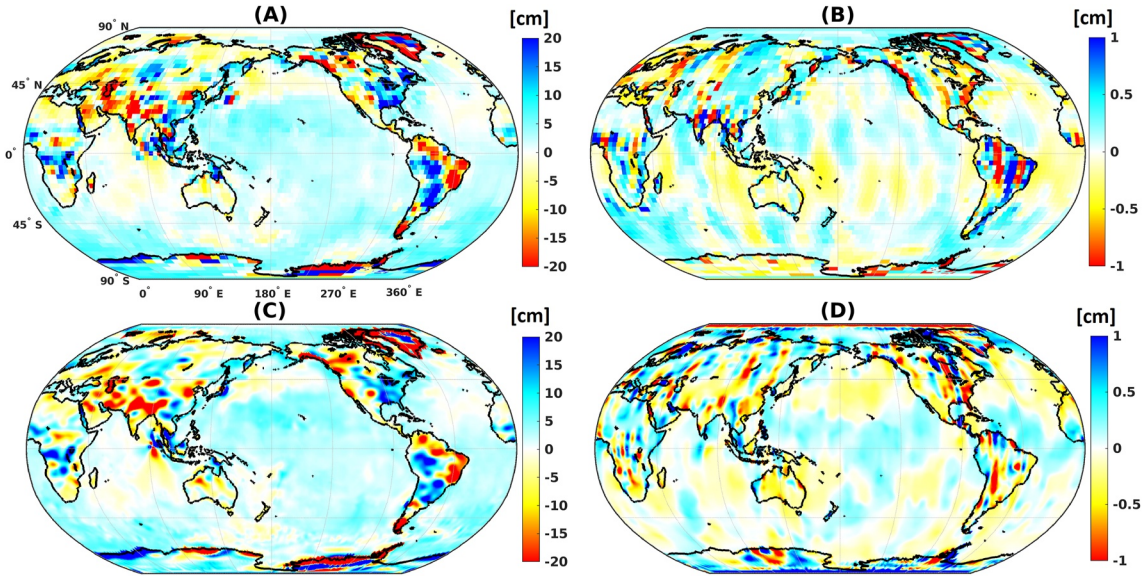

Figure 14. Impact of ACH on GRACE-FO mascon data. GRACE-FO mascon solutions for January 2019 from (a) NASA JPL and (c) NASA GSFC based on the accelerometer transplant data ACT. Update in the mascon solutions caused by the ACH from (b) NASA JPL and (d) NASA GSFC for January 2019.

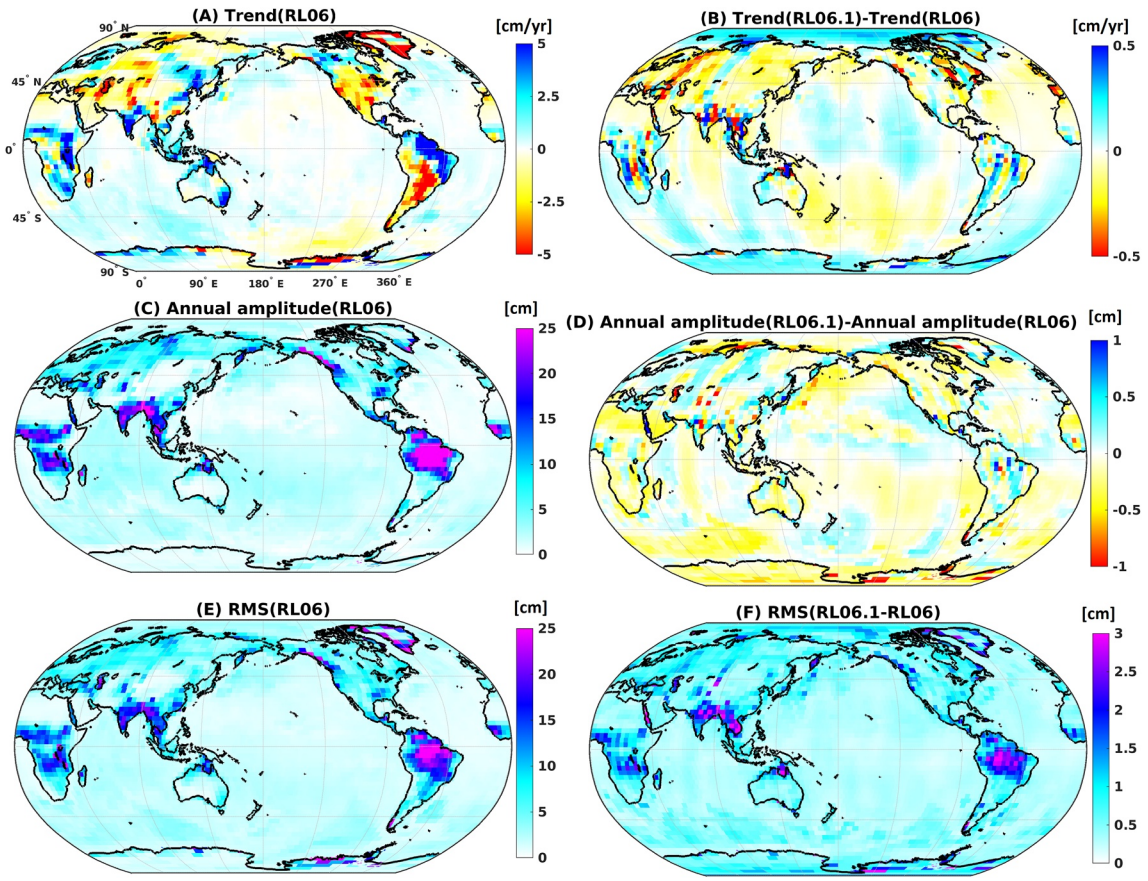

Figure 15. Impact of ACH on GRACE-FO mascon data. (a) Trend, (c) annual amplitude, and (e) RMS variability of GRACE-FO JPL mascon solutions based on ACT for the period from June 2018 to July 2022. Difference between (b) trend and (d) annual amplitude of JPL mascon solutions from ACH and ACT. (f) RMS of difference between mass change timeseries at each grid cell from JPL mascon solutions based on ACT and ACH.

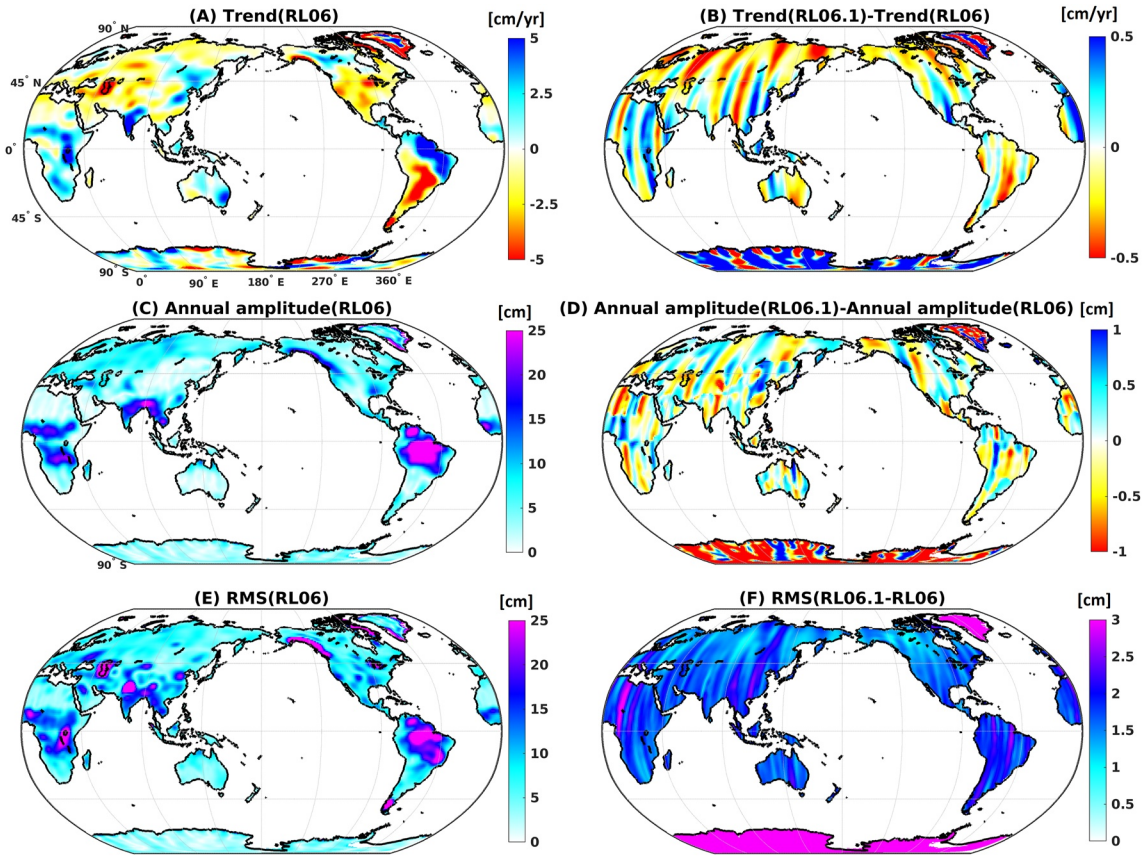

Figure 16. Impact of ACH on GRACE-FO L3 mass change data from GFZ (see http://gravis.gfz-potsdam.de/home). (a) Trend, (c) annual amplitude, and (e) RMS variability of GRACE-FO GFZ L3 mass change data based on ACT for the period from June 2018 to July 2022. Difference between (b) trend and (d) annual amplitude of GFZ L3 mass change data ACH and ACT. (f) RMS of difference between mass change timeseries at each grid cell from GFZ L3 mass change data based on ACT and ACH.

All in all, we find the ACH data product very encouraging because, as our comprehensive analyses show, it leads to improved GRACE-FO time-variable gravity and mass change data. We hope our work (a) helps the SDS centers to evaluate the quality of ACH data product and (b) provides some hints for its further improvement. We will also continue assessing GRACE-FO L2 and L3 data in the future as the solar activity evolves and GRACE-FO altitude decays.

The thrust model used in the new accelerometer transplant data ACH is the same as that used in ACT (McCullough, Harvey, et al., 2022). The thrust model assumes that attitude thruster firings can be modeled by a constant acceleration. As such, it is described by a single value per thruster type and accelerometer direction (Harvey et al., 2022; McCullough et al., 2019). This simplified thrust model is accurate enough for the purpose of monthly time-variable gravity and mass change estimation from GRACE-FO data. However, it causes high-frequency spikes in the LRI ranging residuals, in particular around the Earth's geomagnetic equator. This limits the high-resolution static gravity field analysis from the GRACE-FO LRI data (Ghobadi-Far, Han, McCullough, et al., 2020). Further improvement of the GRACE-FO accelerometer transplant data could also consider improving the thrust model for this purpose.

Data Availability Statement

All the datasets used in this paper are publicly available. GRACE-FO L2 solutions from RL06 and RL06.1: ftp://isdcftp.gfz-potsdam.de/grace-fo/Level-2 and https://search.earthdata.nasa.gov/search?portal=podaac-cloud (search for "Projects: GRACE-FO" and "Processing Levels: 2"). For SDS level-2 data description, see JPL: https://dx.doi.org/10.5067/GFL20-MJ061, CSR: https://dx.doi.org/10.5067/GFL20-MC061, and GFZ:

https://doi.org/10.5880/GFZ.GRACEFO_06_GSM. GRACE-FO JPL mascon solutions from RL06 and RL06.1: https://podaac-tools.jpl.nasa.gov/drive/files/GeodeticsGravity/tellus/L3/mascon. GSFC mascon solutions: https://earth.gsfc.nasa.gov/geo/data/grace-mascons. GFZ GravIS L3 gridded mass change data: http://gravis.gfz-potsdam.de/home. TN-13 and TN-14: https://podaac.jpl.nasa.gov/gravity/gracefo-documentation and ftp://isdcftp.gfz-potsdam.de/grace-fo/DOCUMENTS/TECHNICAL_NOTES. ACH1B: https://search.earthdata.nasa.gov/search?portal=podaac-cloud (search for "Projects: GRACE-FO" and "Processing Levels: 1B"). ICESat-2 data: https://nsidc.org/data/icesat-2/data. CryoSat-2 data: https://earth.esa.int/eogateway/catalog/cryosat-products.

Acknowledgments
We thank Christoph Dahle (GFZ) and Chris McCullough (JPL) for their thoughtful and constructive comments. This work was funded by the National Aeronautics and Space Administration (NASA) Grant 80NSSC21K0061. We thank Veit Helm (Helmholtz Centre for Polar and Marine Research, Alfred Wegener Institute, Bremerhaven, Germany) for providing surface elevation changes derived from CryoSat-2 and ICESat-2. The work of MW and TD was supported by funds of the German Research Foundation (DFG) through Grant HO 4232/4-2 as part of the Special Priority Program 1889 "Regional Sea Level Change and Society" (SeaLevel) and through Grant SCHE 1426/28-1, respectively, as well as by funds of the European Space Agency through the Climate Change Initiative (CCI) projects Antarctic Ice Sheet CCI+ (contract number 4000126813/19/I-NB) and Greenland Ice Sheet CCI+ (contract number 4000126523/19/I-NB).

References

Abich, K., Abramovici, A., Amparan, B., Baatzsch, A., Okihiro, B. B., Barr, D. C., et al. (2019). In-orbit performance of the GRACE follow-on laser ranging interferometer. *Physical Review Letters*, *123*(3), 031101. https://doi.org/10.1103/physrevlett.123.031101

Bandikova, T., McCullough, C., Kruizinga, G. L., Save, H., & Christophe, B. (2019). GRACE accelerometer data transplant. *Advances in Space Research*, *64*(3), 623–644. https://doi.org/10.1016/j.asr.2019.05.021

Behzadpour, S., Mayer-Gürr, T., & Krauss, S. (2021). GRACE Follow-On Accelerometer Data Recovery. *Journal of Geophysical Research: Solid Earth*, *126*(5), e2020JB021297. https://doi.org/10.1029/2020jb021297

Bergmann-Wolf, I., Zhang, L., & Dobslaw, H. (2014). Global eustatic sea-level variations for the approximation of geocenter motion from GRACE. *Journal of Geodetic Science*, *4*(1). https://doi.org/10.2478/jogs-2014-0006

Boergens, E., Kvas, A., Eicker, A., Dobslaw, H., Schawohl, L., Dahle, C., et al. (2022). Uncertainties of GRACE-based terrestrial water storage anomalies for arbitrary averaging regions. *Journal of Geophysical Research: Solid Earth*, *127*(2), e2021JB022081. https://doi.org/10.1029/2021JB022081

Caron, L., Ivins, E. R., Larour, E., Adhikari, S., Nilsson, J., & Blewitt, G. (2018). GIA model statistics for GRACE hydrology, cryosphere, and ocean science. *Geophysical Research Letters*, *45*(5), 2203–2212. https://doi.org/10.1002/2017GL076644

Chen, J., Tapley, B., Seo, K. W., Wilson, C., & Ries, J. (2019). Improved quantification of global mean ocean mass change using GRACE satellite gravimetry measurements. *Geophysical Research Letters*, *46*(23), 13984–13991. https://doi.org/10.1029/2019gl085519

Chen, J., Tapley, B., Tamisiea, M. E., Save, H., Wilson, C., Bettadpur, S., & Seo, K. W. (2021). Error assessment of GRACE and GRACE Follow-On mass change. *Journal of Geophysical Research: Solid Earth*, *126*(9), e2021JB022124. https://doi.org/10.1029/2021jb022124

Dahle, C., Flechtner, F., Murböck, M., Michalak, G., Neumayer, H., Abrykosov, O., et al. (2019). *GRACE-FO D-103919 (Gravity Recovery and Climate Experiment Follow-On), GFZ Level-2 Processing Standards Document for Level-2 Product Release 06 (Rev. 1.0, June 3, 2019). Scientific Technical Report - Data; 19/09*. GFZ German Research Centre for Geosciences. https://doi.org/10.2312/gfz.b103-19098

Ditmar, P. (2022). How to quantify the accuracy of mass anomaly time-series based on GRACE data in the absence of knowledge about true signal? *Journal of Geodynamics*, *96*(8), 54. https://doi.org/10.1007/s00190-022-01640-x

Dobslaw, H., Bergmann-Wolf, I., Dill, R., Poropat, L., Thomas, M., Dahle, C., et al. (2017). A new high-resolution model of non-tidal atmosphere and ocean mass variability for de-aliasing of satellite gravity observations: AOD1B RL06. *Geophysical Journal International*, *211*(1), 263–269. https://doi.org/10.1093/gji/ggx302

Döhne, T., Horwath, M., Groh, A., & Buchta, E. (2023). The sensitivity kernel perspective on GRACE mass change estimates. *Journal of Geodynamics*, *97*(1), 11. https://doi.org/10.1007/s00190-022-01697-8

Flury, J., Bettadpur, S., & Tapley, B. D. (2008). Precise accelerometry onboard the GRACE gravity field satellite mission. *Advances in Space Research*, *42*(8), 1414–1423. https://doi.org/10.1016/j.asr.2008.05.004

Ghobadi-Far, K., Han, S. C., Allgeyer, S., Tregoning, P., Sauber, J., Behzadpour, S., et al. (2020). GRACE gravitational measurements of tsunamis after the 2004, 2010, and 2011 great earthquakes. *Journal of Geodesy*, *94*(7), 1–9. https://doi.org/10.1007/s00190-020-01395-3

Ghobadi-Far, K., Han, S. C., McCullough, C. M., Wiese, D. N., Ray, R. D., Sauber, J., et al. (2022). Along-orbit analysis of GRACE Follow-On inter-satellite laser ranging measurements for sub-monthly surface mass variations. *Journal of Geophysical Research: Solid Earth*, *127*(2), e2021JB022983. https://doi.org/10.1029/2021jb022983

Ghobadi-Far, K., Han, S. C., McCullough, C. M., Wiese, D. N., Yuan, D. N., Landerer, F. W., et al. (2020). GRACE Follow-On laser ranging interferometer measurements uniquely distinguish short-wavelength gravitational perturbations. *Geophysical Research Letters*, *47*(16), e2020GL089445. https://doi.org/10.1029/2020gl089445

Ghobadi-Far, K., Han, S. C., Sauber, J., Lemoine, F., Behzadpour, S., Mayer-Gürr, T., et al. (2019). Gravitational changes of the Earth's free oscillation from earthquakes: Theory and feasibility study using GRACE inter-satellite tracking. *Journal of Geophysical Research: Solid Earth*, *124*(7), 7483–7503. https://doi.org/10.1029/2019jb017530

Ghobadi-Far, K., Han, S. C., Weller, S., Loomis, B. D., Luthcke, S. B., Mayer-Gürr, T., & Behzadpour, S. (2018). A transfer function between line-of-sight gravity difference and GRACE intersatellite ranging data and an application to hydrological surface mass variation. *Journal of Geophysical Research: Solid Earth*, *123*(10), 9186–9201. https://doi.org/10.1029/2018jb016088

Ghobadi-Far, K., Šprlák, M., & Han, S. C. (2019). Determination of ellipsoidal surface mass change from GRACE time-variable gravity data. *Geophysical Journal International*, *219*(1), 248–259. https://doi.org/10.1093/gji/ggz292

Groh, A., & Horwath, M. (2021). Antarctic Ice mass change products from GRACE/GRACE-FO using tailored sensitivity kernels. *Remote Sensing*, *13*(9), 1736. https://doi.org/10.3390/rs13091736

Groh, A., Horwath, M., Horvath, A., Meister, R., Sørensen, L. S., Barletta, V. R., et al. (2019). Evaluating GRACE mass change time series for the Antarctic and Greenland Ice Sheet—Methods and results. *Geosciences*, *9*(10), 415. https://doi.org/10.3390/geosciences9100415

Han, S. C., Ghobadi-Far, K., Ray, R. D., & Papanikolaou, T. (2020). Tidal geopotential dependence on Earth ellipticity and seawater density and its detection with the GRACE Follow-On Laser Ranging Interferometer. *Journal of Geophysical Research: Oceans*, *125*(12), e2020JC016774. https://doi.org/10.1029/2020jc016774

Han, S. C., Ghobadi-Far, K., Yeo, I. Y., McCullough, C. M., Lee, E., & Sauber, J. (2021). GRACE Follow-On revealed Bangladesh was flooded early in the 2020 monsoon season due to premature soil saturation. *Proceedings of the National Academy of Sciences*, *118*(47), e2109086118. https://doi.org/10.1073/pnas.2109086118

Han, S. C., Shum, C. K., Bevis, M., Ji, C., & Kuo, C. Y. (2006). Crustal dilatation observed by GRACE after the 2004 Sumatra-Andaman earthquake. *Science*, *313*(5787), 658–662. https://doi.org/10.1126/science.1128661

Han, S. C., Yeo, I. Y., Khaki, M., McCullough, C. M., Lee, E., & Sauber, J. (2021). Novel Along-Track Processing of GRACE Follow-On Laser Ranging Measurements Found Abrupt Water Storage Increase and Land Subsidence During the 2021 March Australian Flooding. *Earth and Space Science*, *8*(11), e2021EA001941. https://doi.org/10.1029/2021ea001941

Harvey, N., McCullough, C. M., & Save, H. (2022). Modeling GRACE-FO accelerometer data for the version 04 release. *Advances in Space Research*, *69*(3), 1393–1407. https://doi.org/10.1016/j.asr.2021.10.056

Helm, V., Humbert, A., & Miller, H. (2014). Elevation and elevation change of Greenland and Antarctica derived from CryoSat-2. *The Cryosphere*, *8*(4), 1539–1559. https://doi.org/10.5194/tc-8-1539-2014

Howat, I. M., Porter, C., Smith, B. E., Noh, M.-J., & Morin, P. (2019). The Reference Elevation Model of Antarctica. *The Cryosphere*, *13*(2), 665–674. https://doi.org/10.5194/tc-13-665-2019

Ivins, E. R., James, T. S., Wahr, J., Schrama, E. J. O., Landerer, F. W., & Simon, K. M. (2013). Antarctic contribution to sea level rise observed by GRACE with improved GIA correction. *Journal of Geophysical Research: Solid Earth*, *118*(6), 3126–3141. https://doi.org/10.1002/jgrb.50208

Jekeli, C. (1981). Alternative methods to smooth the Earth's gravity field (No. NASA-CR-168758).

Kaula, W. M. (1966). *Theory of satellite geodesy*. Blaisdel Publishing Company.

Kim, J. R. (2000). *Simulation study of a low-low satellite-to-satellite tracking mission* (Dissertation). University of Texas at Austin.

Kvas, A., Behzadpour, S., Ellmer, M., Klinger, B., Strasser, S., Zehentner, N., & Mayer-Gürr, T. (2019). ITSG-Grace2018: Overview and evaluation of a new GRACE-only gravity field time series. *Journal of Geophysical Research: Solid Earth*, *124*(8), 9332–9344. https://doi.org/10.1029/2019jb017415

Landerer, F., Flechtner, F., Save, H., McCullough, C. M., Dahle, C., Bettadpur, S., et al. (2022). Extending Global Mass Change Satellite Observations Into the Third Decade With GRACE-FO: Science Mission Status and Plans. In *GRACE/GRACE-FO Science Team Meeting, Potsdam, Germany, 18–20 October 2022*.

Landerer, F. W., Flechtner, F. M., Save, H., Webb, F. H., Bandikova, T., Bertiger, W. I., et al. (2020). Extending the global mass change data record: GRACE Follow-On instrument and science data performance. *Geophysical Research Letters*, *47*(12), e2020GL088306. https://doi.org/10.1029/2020GL088306

Ligtenberg, S. R. M., Helsen, M. M., & van den Broeke, M. R. (2011). An improved semi-empirical model for the densification of Antarctic firn. *The Cryosphere*, *5*(4), 809–819. https://doi.org/10.5194/tc-5-809-2011

Loomis, B. D., Luthcke, S. B., & Sabaka, T. J. (2019). Regularization and error characterization of GRACE mascons. *Journal of Geodesy*, *93*(9), 1381–1398. https://doi.org/10.1007/s00190-019-01252-y

Loomis, B. D., Rachlin, K. E., & Luthcke, S. B. (2019). Improved Earth oblateness rate reveals increased ice sheet losses and mass-driven sea level rise. *Geophysical Research Letters*, *46*(12), 6910–6917. https://doi.org/10.1029/2019gl082929

Loomis, B. D., Rachlin, K. E., Wiese, D. N., Landerer, F. W., & Luthcke, S. B. (2020). Replacing GRACE/GRACE-FO C30 with satellite laser ranging: Impacts on Antarctic Ice Sheet mass change. *Geophysical Research Letters*, *47*(3), e2019GL085488. https://doi.org/10.1029/2019GL085488

Martín-Español, A., Bamber, J. L., & Zammit-Mangion, A. (2017). Constraining the mass balance of East Antarctica. *Geophysical Research Letters*, *44*(9), 4168–4175. https://doi.org/10.1002/2017GL072937

McCullough, C. M., Fahnestock, E. G., Wiese, D. N., & Yuan, D.-N. (2022). *JPL Level-2 GRACE-FO Products - Release Notes Version 6.1. Jet Propulsion Laboratory*. California Institute of Technology. Retrieved from https://podaac-tools.jpl.nasa.gov/drive/files/GeodeticsGravity/gracefo/docs/GRACE-FO_L2-ReleaseNotes_JPL_RL06.1.pdf

McCullough, C. M., Harvey, N., Save, H., & Bandikova, T. (2019). *Description of calibrated GRACE-FO Accelerometer Data Products*. Jet Propulsion Laboratory, California Institute of Technology, Technical Report JPL D-103863. Retrieved from https://podaac-tools.jpl.nasa.gov/drive/files/allData/gracefo/docs/GFO.ACT.JPL-D-103863.20190520.pdf

McCullough, C. M., Harvey, N., Save, H., Miller, M. A., Bertiger, W., Yuan, D.-N., & Landerer, F. W. (2022). Operational GRACE-FO Accelerometer Transplant Strategies. In *AGU Fall Meeting 2022. Chicago, USA, 12-16 December 2022*.

Ray, R. D., Luthcke, S. B., & Boy, J. P. (2009). Qualitative comparisons of global ocean tide models by analysis of intersatellite ranging data. *Journal of Geophysical Research*, *114*(C9), C09017. https://doi.org/10.1029/2009jc005362

Ries, J., Bettadpur, S., Eanes, R., Kang, Z., Ko, U. D., McCullough, C., et al. (2016). *The development and evaluation of the global gravity model GGM05. Technical Memorandum CSR-TM-16-01*. Center for Space Research of University of Texas. Retrieved from https://repositories.lib.utexas.edu/handle/2152/74341

Rodell, M., Famiglietti, J. S., Wiese, D. N., Reager, J. T., Beaudoing, H. K., Landerer, F. W., & Lo, M. H. (2018). Emerging trends in global freshwater availability. *Nature*, *557*(7707), 651–659. https://doi.org/10.1038/s41586-018-0123-1

Sasgen, I., Groh, A., & Horwath, M. (2019). *GFZ GravIS RL06 Ice-Mass Change Products. V. 0003*. GFZ Data Services. https://doi.org/10.5880/GFZ.GRAVIS_06_L3_ICE

Save, H., Bettadpur, S., & Tapley, B. D. (2016). High-resolution CSR GRACE RL05 mascons. *Journal of Geophysical Research: Solid Earth*, *121*(10), 7547–7569. https://doi.org/10.1002/2016jb013007

Save, H. V., Bettadpur, S. V., & Tapley, B. D. (2006). Single accelerometer gravity solutions for GRACE. In *AGU Fall Meeting Abstract* (pp. G13A–0026).

Shepherd, A., Ivins, E., Rignot, E., Smith, B., van den Broeke, M., & Velicogna, I. (2020). Mass balance of the Greenland Ice Sheet from 1992 to 2018. *Nature*, *579*(7798), 233–239. https://doi.org/10.1038/s41586-019-1855-2

Shepherd, A., Ivins, E., Rignot, E., Smith, B., van den Broeke, M., Velicogna, I., et al. (2018). Mass balance of the Antarctic Ice Sheet from 1992 to 2017. *Nature*, *558*(7709), 219–222. https://doi.org/10.1038/s41586-018-0179-y

Sun, Y., Riva, R. E. M., & Ditmar, P. (2016). Optimizing estimates of annual variations and trends in geocenter motion and J2 from a combination of GRACE data and geophysical models. *Journal of Geophysical Research: Solid Earth*, *121*(11), 8352–8370. https://doi.org/10.1002/2016JB013073

Swenson, S., Chambers, D., & Wahr, J. (2008). Estimating geocenter variations from a combination of GRACE and ocean model output. *Journal of Geophysical Research*, *B113*(B8), B08410. https://doi.org/10.1029/2007JB005338

Swenson, S., & Wahr, J. (2006). Post-processing removal of correlated errors in GRACE data. *Geophysical Research Letters*, *33*(8), L08402. https://doi.org/10.1029/2005gl025285

Tapley, B. D., Bettadpur, S., Ries, J. C., Thompson, P. F., & Watkins, M. M. (2004). GRACE measurements of mass variability in the Earth system. *Science*, *305*(5683), 503–505. https://doi.org/10.1126/science.1099192

Tapley, B. D., Watkins, M. M., Flechtner, F., Reigber, C., Bettadpur, S., Rodell, M., et al. (2019). Contributions of GRACE to understanding climate change. *Nature Climate Change*, *9*(5), 358–369. https://doi.org/10.1038/s41558-019-0456-2

van Wessem, J. M., van de Berg, W. J., Noël, B. P. Y., van Meijgaard, E., Amory, C., Birnbaum, G., et al. (2018). Modelling the climate and surface mass balance of polar ice sheets using RACMO2 – Part 2: Antarctica (1979–2016). *The Cryosphere*, *12*(4), 1479–1498. https://doi.org/10.5194/tc-12-1479-2018

Wahr, J., Molenaar, M., & Bryan, F. (1998). Time variability of the Earth's gravity field: Hydrological and oceanic effects and their possible detection using GRACE. *Journal of Geophysical Research*, *103*(B12), 30205–30229. https://doi.org/10.1029/98JB02844

Watkins, M. M., Wiese, D. N., Yuan, D. N., Boening, C., & Landerer, F. W. (2015). Improved methods for observing Earth's time variable mass distribution with GRACE using spherical cap mascons. *Journal of Geophysical Research: Solid Earth*, *120*(4), 2648–2671. https://doi.org/10.1002/2014jb011547

Willen, M. O., Horwath, M., Groh, A., Helm, V., Uebbing, B., & Kusche, J. (2022). Feasibility of a global inversion for spatially resolved glacial isostatic adjustment and ice sheet mass changes proven in simulation experiments. *Journal of Geodynamics*, *96*(10), 1–21. https://doi.org/10.1007/s00190-022-01651-8

Yuan, D.-N. (2019). *Gravity Recovery and Climate Experiment Follow-On: Level-2 Gravity Field Product User Handbook*. Jet Propulsion Laboratory, California Institute of Technology. Retrieved from https://podaac-tools.jpl.nasa.gov/drive/files/allData/gracefo/docs/GRACE-FO_L2_UserHandbook.pdf

Zwally, H. J., Giovinetto, M. B., Beckley, M. A., & Saba, J. L. (2012). *Antarctic and Greenland Drainage Systems*. GSFC Cryospheric Sciences Laboratory. Retrieved from https://earth.gsfc.nasa.gov/cryo/data/polar-altimetry/antarctic-and-greenland-drainage-systems